Implementation of hydrodynamic forces into the Moving Frame Method for analysis of multi-body wave energy converters

Joakim Nyland

Master's Thesis in Ocean Technology

June 2020

Department of Physics and Technology

University of Bergen

ABSTRACT

The aim of this research is to implement hydrodynamic forces into the Moving Frame Method (MFM) to enable time-dependent analysis of multi-body wave energy converters in irregular sea-states.

The MFM leverages Lie Group Theory, Cartan's concept of moving frames, and Frankel's compact notation from the discipline of geometrical physics. Furthermore, it makes use of a coherent data structure founded in the Special Euclidean Group SE(3). Together these implementations maintain a notation which is consistent from 2D to 3D single bodies to multi-bodies, allowing for analysis which can be readily scaled up to include multiple links, bodies, and farms of devices, without increasing notational complexity and without loss of generality.

This work models the three-float M4 WEC subject to irregular wave spectra using the MFM and linearization by Cummins' equation. The impulse response function is pre-computed, and the hydrodynamic coefficients are taken from a WAMIT diffraction model. The power-take-off (PTO) is modelled as a linear damper. The system of second-order ordinary differential equations is advanced in time using the fourth order Runge-Kutta numerical method.

Model-scale results are compared to earlier experimental work and show close agreement, with root-mean square errors of the time-series heave and surge responses less than 4×10^{-3} m. Power capture and θ_{rms} show close agreement across all peak periods with only a slight underprediction (<7%) of power at peak periods shorter than 1 s. Some discrepancies between the model-scale results and earlier experimental work are found and this is attributed to moments from the WAMIT diffraction model being generated about the centre of flotation and not the centre of mass, which is required in an MFM model. Full-scale results of annual energy yield for a wave site in Ireland show only a minor underprediction (<3%) compared to an earlier vectorial mechanics model.

The results validate that hydrodynamic forces have been successfully implemented into the MFM model, opening for analysis of more complex wave energy converters with higher degrees of freedom, including other multi-body marine devices.

SAMMENDRAG

Målet med denne masteroppgaven er å implementere hydrodynamiske krefter til Moving Frame metoden (MFM) for å muliggjøre tidsavhengige analyser av komplekse bølgeenergi-kraftverk i irregulære sjøtilstander.

MFM er en ny metode innenfor dynamikk som utnytter Lie Group Theory, Cartans konsept med bevegelige rammer og Frankels kompakte notasjon fra geometrisk fysikk. Metoden benytter seg også av en kompakt datastruktur fra Special Euclidean Group SE(3). Dette opprettholder en notasjon som er konsistent fra 2D- og 3D-enkeltlegemer til flerlegemer, noe som muliggjør en analyse som lett kan skaleres opp til å inkludere flere koblinger, legemer og grupper av enheter uten å øke notasjonskompleksiteten.

Dette masterprosjektet modellerer et M4 bølgekraftverk i irregulære sjøtilstander ved å benytte MFM og linearisering ved hjelp av Cummins ligning. Impulsresponsfunksjonen forhåndsberegnes og hydrodynamiske koeffisienter hentes ut fra en WAMIT diffraksjonsmodell. Kraftuttaket (PTO) modelleres som en lineær demper. Systemet av andre ordens differensialligninger løses ved bruk av fjerdeordens Runge-Kutta-metode.

Modell-skala resultat sammenlignes med tidligere eksperimenter på samme oppsett og viser god overensstemmelse med *root-mean square error* av responsen for hiv og jag på mindre enn 4×10^{-3} m. Kraftgenerering og θ_{rms} viser god overensstemmelse over hele spekteret av perioder med bare en liten underestimering (<7%) av kraft for perioder kortere enn 1 s. Det er noen små avvik mellom modell-skala resultatene og tidligere eksperimenter på grunn av WAMIT-diffraksjonsmodellen som genereres om flotasjonssenter og ikke massesenter, som kreves i en MFM-modell. Full-skala resultat av årlig kraftgenerering for en lokasjon i Irland viser en mindre underestimering (<3%) sammenlignet med en gammel vektormekanikk modell.

Resultatene validerer at hydrodynamiske krefter er riktig implementert i MFM-modellen noe som muliggjør analyse av mer komplekse bølgeenergi-kraftverk og andre marine enheter i alle seks frihetsgrader.

PREFACE

The master thesis is written as part of a two years master's programme in Ocean Technology at the University of Bergen and Western Norway University of Applied Sciences (HVL). The main topics in this thesis concern marine technology and hydrodynamics with Prof. Thomas J. Impelluso and Dr. David R. Lande-Sudall as internal supervisors. The master student has a bachelor's degree in Subsea Engineering and has previously researched relevant topics such as *Minimising Motions of Floating Vessels Using the Moving Frame Method in Dynamics* [1] and *Dual Gyroscope Wave Energy Converter* [2].

I extend my thanks to Thomas and David for being the mentors from HVL. Thomas Impelluso has provided expertise on the Moving Frame Method and David Lande-Sudall has provided great help on hydrodynamics and coding. Also, thanks to Bjørn Tore Hjertaker for being a helpful and supportive mentor from the University of Bergen.

Thanks to Prof. Peter Stansby, University of Manchester, for providing WAMIT hydrodynamic coefficients and results from his vectorial mechanics model and experimental tests [3].

Finally, thanks to HVL and the University of Bergen for five years of education.

TABLE OF CONTENTS

LIST OF FIGURES

LIST OF TABLES

1 INTRODUCTION

This project analyses a new type of wave energy generator for clean energy, in compliance with the European Union's target of becoming climate-neutral by 2050; an objective at the heart of the European Green Deal and in line with the global Paris Agreement [4]. The EU is committed towards implementing the United Nation's Agenda for Sustainable Development [4]. This agenda is based upon the UN's 17 Sustainable Development Goals (SDGs) [5]. The SDGs are a transformative roadmap for national and international efforts aimed at eradicating extreme poverty while protecting planetary boundaries and promoting prosperity, peace, and justice. This master project addresses several of these, focusing mostly on goal 7: affordable and clean energy.

The ocean contains vast amounts of wave energy and devices for harnessing this energy have been investigated since the late 1970's [6] with many technologies being proposed [7]. Many devices did not survive the harsh ocean environment, whilst others have shown low power capture for real broadband sea spectra, for example [8-13]. One device which has shown promise for overcoming these issues, and the focus of this study, is the Multi-Mode Moored Multibody device, known as M4 [3] (see Figure 1). The multiple floats give a broadband frequency response, allowing power capture in a wider range of sea-states than devices based on single bodies. Several such devices can be assembled to create a "farm" with the intention of increasing power output. Aside from large grid-based generation, other possible uses are energy for aquaculture (e.g. fish farming), offshore weather stations, subsea equipment and supplemental power for oil and gas platforms.

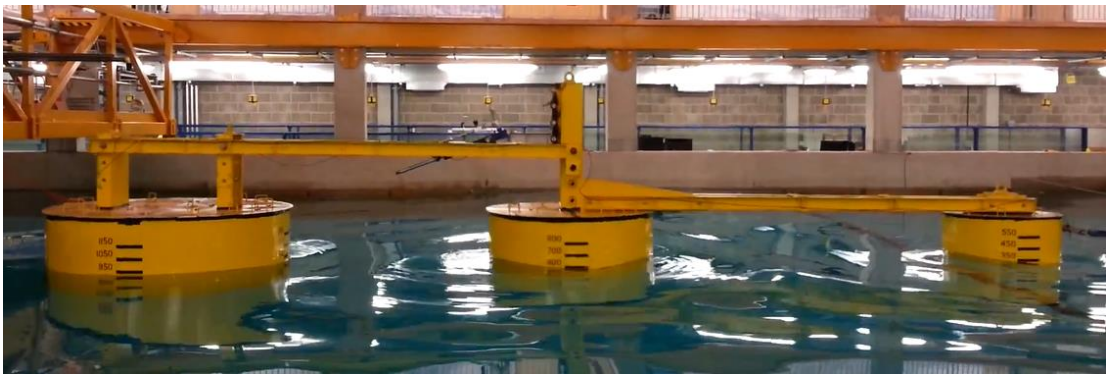

Figure 1. Photography of the M4 wave energy converter [14].

Analysing the hydrodynamics of wave energy converters (WECs) is a non-trivial task due to the complexity of the interacting forces that take place. In order to model energy capture from such devices, linear hydrodynamic theory is often used [15]. This can be conducted in the frequency domain, but it is of interest to study devices in the time-domain due to phase-dependent effects.

Existing methods in dynamics, while reliable, are not readily extensible due to problematic aspects in modelling, e.g. with respect to spatial rotations. The power of the Moving Frame Method (MFM) is to extract equations of motion from multi-body spatial systems, while maintaining a notation that is consistent from 2D and 3D single-bodies to multi-bodies. The MFM replaces an inordinate reliance on vector algebra with the framework of Lie algebra reduced to the simplicity of rotation matrices. This allows the equations of motion to be delivered in a way suitable for rapid software deployment and for use in power control systems. This enables efficient optimisation of the M4 device arrangements and float sizes relative to the site-specific resource.

The specific objectives of this master project are to:

1) Implement hydrodynamic forces into the MFM in order to solve the equations of motion of multi-body WECs in irregular sea-states for the first time with this method.
2) Validate the MFM model by modelling a three-float M4 WEC in irregular sea-states and compare the results to an experimentally-validated vectorial mechanics model from [3].

Section 2 prepares for analysis in irregular sea states and reviews several methods of harnessing energy from waves. Following, section 3 introduces and summarises the MFM. Sections 4 and 5 present the dynamics and kinetics of the M4 device, respectively. Next, section 6 introduces the hydrodynamics and presents the code structure. Section 7 presents the results in comparison with prior research of [3]. Finally, section 8 and 9 conclude the thesis with suggestions of future work.

2 WAVE ENERGY CONVERTERS

There have been many different attempts in extracting energy successfully from waves, e.g. as presented in [8-13]. Wave energy technology has not yet found a standardised solution in harvesting the wave power. There are two main reasons why so many attempts have resulted in failure;

1) survivability, and
2) economically effective energy extraction from a broadband frequency spectrum.

Designs vary from one wave energy converter (WEC) to another, mainly due to differences in water depth, location and working principle. Several methods have been proposed to classify wave energy systems. Figure 2 shows one such classification from [16], classifying WECs based mostly on working principles; oscillating water-, overtopping- and oscillating body converters.

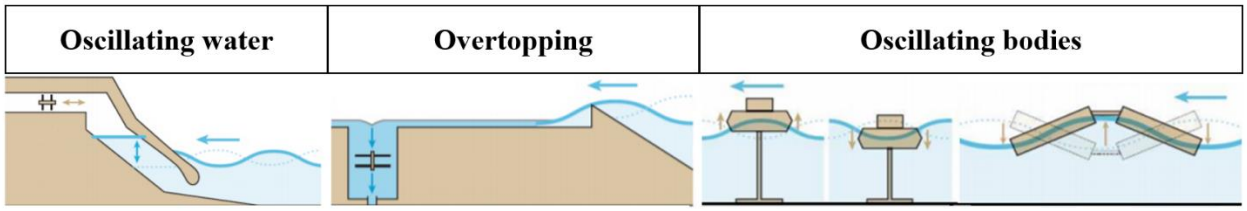

Figure 2. Wave energy converters based on working principle [16]

To describe WECs, a commonly used term is *rated power*, i.e. the theoretical maximum power capacity at which the equipment has been designed to operate.

The capacity of a WEC is usually sized for mean wave conditions where power is typically generated. Consequently, a big challenge with wave energy is how to protect WECs from extreme waves that they are not designed to handle. A device generally spends much of the time generating less than rated power, it might also be able to handle generating a little more power, but it should handle any amount up to the rated power and perform as expected. The absorbed energy is transformed into useable electricity through a power take-off (PTO) mechanism of the WEC. The following subchapters briefly introduces some attempts in extracting energy from waves.

2.1 Oscillating Water Column Converters

An oscillating water column converter (to the left in Figure 2) works on the principle of wave induced air pressurisation. The device consists of a closed air chamber above the water, and the oscillating column of water increases and decreases the air pressure within the chamber as the level

rises and falls. This causes air to flow through a turbine that drives an electrical generator. Rated power of such a converter is usually in the range 60–500 kW [7]. An example of an oscillating water column converter is the Norwegian Kvaerner Multiresonant OWC. A 500-kW demonstration plant based on this concept was built outside Bergen, Norway [8]. Another example of an oscillating water column converter is Mighty Whale (rated power of 110 kW), as shown in the photography in Figure 3 [9].

Figure 3. Photography of the Mighty Whale [17]

2.2 Overtopping Converters

Overtopping converters (the middle illustration in Figure 2) capture the water that over spills into a reservoir. The potential energy of the stored water is converted into useful energy through a hydraulic turbine which runs an electric generator. An example of an overtopping converter is the Norwegian Tapchan. A prototype (rated power of 350 kW) of the Norwegian Tapchan was built in 1985 outside Bergen, Norway [8]. Another example of an overtopping converter is the Wave Dragon (rated power of 4-10 MW), as shown in the photography in Figure 4. A 57 m-wide prototype of the Wave Dragon was developed and deployed in Denmark and connected to the grid in 2003 as the world's first offshore grid-connected wave energy device [10]. Concession to build a 7 MW demonstration project of the Wave Dragon in Wales is currently being sought [18].

Figure 4. Photography of Wave Dragon [10]

2.3 Oscillating Body Systems

The basic principle of wave energy exploitation for oscillating bodies (to the right in Figure 2) is that destructive interference must be created between the incident wave and the motion of the WEC. An oscillating WEC is characterised by specific natural periods and when the incident wave period matches the WEC's natural period, resonance occurs and the maximum possible energy is absorbed. Oscillating body systems usually exploit the more powerful wave regimes available in deep water. Complexity, together with additional problems associated with mooring, access for maintenance and the need of long underwater electrical cables, has hindered their development [7]. Below are some examples of oscillating body systems, split into heaving and pitching devices.

Heaving devices

The simplest oscillating body system is the heaving buoy reacting against a fixed frame of reference. The relative wave-induced heave motion between the float and the fixed frame of reference activates a PTO system and drives a linear electric generator [7]. A 10 kW rated power prototype L-10 was deployed and tested in USA, September 2008 [19]. Several other examples of single-body and two-body heaving buoys are listed in [7], for example G-1T, the Norwegian power buoy (shown in Figure 5), AquaBuoy, IPS Buoy, FO3, Wavebob (shown in Figure 6) and PowerBuoy.

Figure 5. Photography of Norwegian power buoy [20]

Figure 6. Photography of Wavebob [21]

Pitching devices

An oscillating body system can exploit rotational motion for power extraction; it is the pitching motion of the device that activates the PTO system. An example of a pitching device is Pelamis, as

shown in the photography in Figure 7. Pelamis (rated power of 750 kW) is a snake-like structure composed of four cylindrical sections linked by hinged joints. The wave induced bending motion of these joints is resisted by hydraulic rams, which pump high-pressure oil through hydraulic motors driving three electrical generators [12]. In 2008, a set of three Pelamis devices was deployed off the Portuguese northern coast, but the waves eventually caused leaks in the buoyancy tanks. Several technical problems followed, and Pelamis lost its financial backing [22].

Salter's Duck, as illustrated in Figure 8, is another oscillating body system that exploits wave induced pitching motion (rated power of 10 kW) [13]. Salter's Duck consists of gyroscopes and exploits the gyroscopic effect for power extraction. One more example of a gyroscopic WEC is the Wello Penguin [23] which was grid-connected at the European Wave Energy Centre, EMEC in Orkney, Scotland. A similar example is a dual gyroscopic wave energy converter that uses spinning gyroscopes and pitching motion of a buoy to generate electricity. The dual gyroscopic wave energy converter is analysed using the MFM (in regular sea-conditions) by the author in [2] but only considering buoyancy forces.

Figure 7. Photography of Pelamis [12]

Figure 8. Salter's Duck [24]

Multi-Mode Moored Multibody device

One method which shows promise for surviving in harsh weather and capturing power across a broadband frequency spectrum is the Multi-Mode Moored Multibody (M4) device [3], which is the focus of this study. The device exploits several modes of motion from the predominant wave-induced motions in heave, surge, and pitch. This study uses the MFM to conduct an analysis of a 111-configuration of the M4. The 111-terminology that prefaces the M4 indicates that there is one stern float, one mid float and one bow float, as shown in Figure 9. There are several other possible configurations of the device, for example 123, 133, 134 configurations and more [3]. The increased

numbers of float configurations give impetus for having a method which is readily scaled up to several floats.

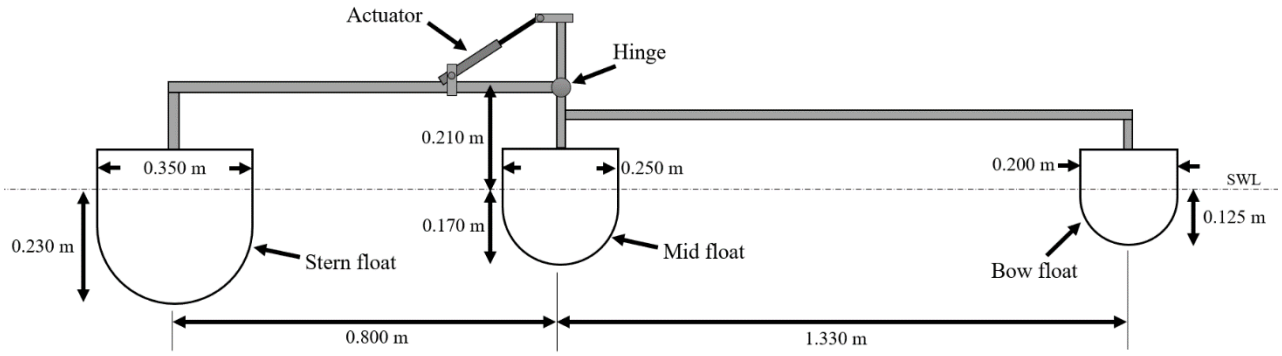

Figure 9. Schematic of the model-scale M4 WEC showing overall dimensions.

The floats are circular in cross section with rounded bases to minimise drag losses. Size decreases from stern to bow; this provides a range of natural periods in heave and pitch. In other words, a range of natural periods in heave and pitch results in a broadband response, meaning that there is a significant variation of response for several different sea conditions. Furthermore, these motions are all coupled so that they help to excite one another. The distance between floats is about half a typical wavelength so that forces and adjacent float motions are predominantly in anti-phase [3].

From the stern float (largest, on the left in Figure 9) a rigid structure (dark grey elements) connects to a hinge point above the mid float. This allows for the rotation that, in turn, activates the power take-off mechanism. In this way, mechanical energy is transformed into useable electricity by extension and compression of the actuator – such as a linear generator or a hydraulic-accumulator system.

The M4 could be a significant contributor to renewable energy generation from waves if:

1. it proves to have high survivability in harsh weather (this has been demonstrated to some extent by experimental testing in [3])
2. it is proven to have effective energy extraction for a broadband frequency spectrum.

It is imperative to find optimal device arrangements and float sizes relative to the site-specific resource. Such optimisation requires rapid calculation of many device layouts. The extensibility of the MFM may enable such studies.

2.4 Analysis in irregular sea states

The development of a WEC from an original idea to a marketable product involves a series of test stages including; concept validation, design validation, system validation, and prototype demonstration [25]. In the first stages of the process, a small-scale model of the device is used. Performance of WECs are normally scaled up from the model-scale to full-scale by applying Froude's similitude law [25]. Froude similitude requires dynamic similarity where the inertial, F_i, and gravitational forces, F_g, which gives the Froude number, F_r (eqn. (1)), is constant between model and full scale.

$$F_r = \frac{F_i}{F_g} = \frac{\rho \frac{V^2}{L}}{\rho g} = \frac{V}{\sqrt{gL}} \tag{1}$$

V is the velocity of the device, ρ is density and L is length in eqn. (1).

To achieve similitude, the model-scale device and the full-scale device also require geometric and kinematic similarities. Froude scaling is typically used for experiments of fluids with a free surface, where gravitational forces are important. An alternative force relationship is that between the inertial force and viscous force, i.e. Reynold's number. This is important where viscous effects and turbulence are significant, but Reynold's scaling is generally difficult to achieve in practice. Using scaling by Froude's number, units such as metres, kilograms, Newtons and seconds are scaled by using a geometric scaling factor, λ, i.e. the ratio of full to model scale dimensions. Of relevance in this work is to find the power capture for the full-scale device, P_s, from the model-scale device, P_m:

$$P_s = P_m \lambda^{3.5} \frac{\rho_s}{\rho_m} \tag{2}$$

where ρ_S and ρ_M are the density in sea- and fresh water, respectively. The significant wave height (mean of the highest one-third of all waves), H_S, and peak wave period, T_P, are also scaled using λ, where the subscript m is related to the model-scale and s is related to the full-scale model.

$$H_{Ss} = H_{Sm}\lambda \tag{3}$$

$$T_{Ps} = T_{Pm}\sqrt{\lambda} \tag{4}$$

This work analyses WECs in irregular sea states for unidirectional waves. Short term stationary irregular sea states may be described by a wave spectrum, i.e. the power spectral density function of the vertical sea surface displacement [26]. The spectral density function explains how the energy is distributed over a range of frequencies. The JOint North Sea WAve Project (JONSWAP) spectrum and the Pierson-Moskowitz spectrum are frequently applied. The Pierson-Moskowitz spectrum is generally applied for open, deep waters and fully developed seas, while the JONSWAP spectrum is normally used for fetch-limited, developing seas and without swell [26]. The input wave spectrum is defined by its significant wave height and angular spectral peak frequency, ω_p [26]:

$$S(\omega) = \alpha g^2 (2\pi)^{-4} \omega^{-5} \exp\left[-\frac{5}{4}\left(\frac{\omega}{\omega_p}\right)^{-4} + e^{-\frac{1}{2}\left(\frac{\omega-\omega_p}{\sigma\omega_p}\right)^2} \ln(\gamma)\right] \tag{5}$$

where

$\omega = angular\ wave\ frequency, \omega = 2\pi f$,
$f = wave\ frequency, f = 1/T$,
$T = wave\ period$,
$\omega_p = angular\ spectral\ peak\ frequency, \omega_p = 2\pi f_p$,
$g = acceleration\ of\ gravity$,
$\sigma = spectral\ width\ parameter, \left(0.07\ if\ \omega \leq \omega_p\right)$ & $\left(0.09\ if\ \omega > \omega_p\right)$,
$\gamma = peakedness\ parameter$, (Pierson-Moskowitz = 1) & (JONSWAP = 3.3),
$\alpha = \frac{5}{16}\frac{H_s^2 \omega_p^4}{g^2}(1 - 0.287\ln(\gamma))$,

The wave spectrum for three different peak periods is plotted in Figure 10 for a typical peakedness parameter $\gamma = 3.3$ [26].

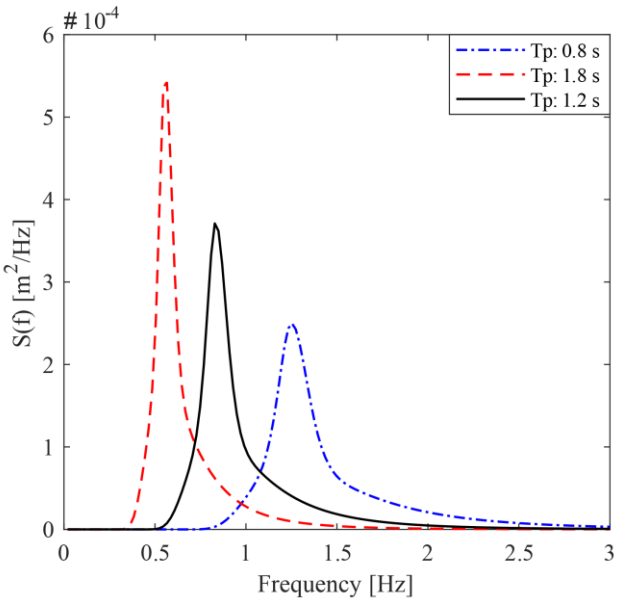

Figure 10. JONSWAP wave spectra for $H_s = 0.04\ m$, $\gamma = 3.3$

The amplitude of the wave spectra is:

$$\xi_A(\omega) = \sqrt{2S(f)df} \tag{6}$$

where *df* is the frequency step size (defined in this work as a set of 200 frequency intervals evenly spaced between 0 and 4 Hz).

In order to establish a suitable rated power for a device, energy capture for various sites is first computed by using a probability of occurrence scatter diagram. The scatter diagram, here from Belmullet in Ireland [27] as shown in Table 1, shows how frequently combinations of H_s and the average zero-crossing wave period, T_z, occur throughout a year. The peak period is related to the average zero-crossing wave period [26]:

$$T_z = T_p \left(\frac{5+\gamma}{11+\gamma}\right)^{1/2} \tag{7}$$

Table 1. Wave occurrence scatter diagram from Belmullet in Ireland [27].

	Period (T_z)												
		1	2	3	4	5	6	7	8	9	10	11	12	13
Heights (H_s)	Ireland													
	0.5				17	39	13	0	0	0	4	0	0	0
	1				148	312	93	32	13	0	1	0	0	0
	1.5				75	560	372	187	64	11	2	0	0	0
	2				6	427	623	321	172	47	8	0	0	0
	2.5					99	508	363	182	67	10	0	0	0
	3					10	248	394	193	83	18	2	0	0
	3.5						86	436	244	74	15	7	1	1
	4						14	213	246	97	23	7	8	0
	3.5							83	218	124	22	4	3	2
	4							17	175	118	26	3	5	3
	4.5								88	122	36	2	1	0
	6								30	86	37	3	3	0
	6.5									45	32	4	4	1
	7									24	48	15	4	0
	7.5									9	30	10	2	0
	8									2	20	16	4	0
	8.5										10	9	7	0
	9										5	18	1	2
	9.5										2	8	2	0
	10										1	4	0	1
	10.5											1	0	0

Figure 11 shows the occurrences of peak energy periods for the site in Table 1, where peak energy period is defined as $T_e = 0.84T_P$ for $\gamma = 3.3$ (note $T_e = 0.78T_P$ for $\gamma = 1$).

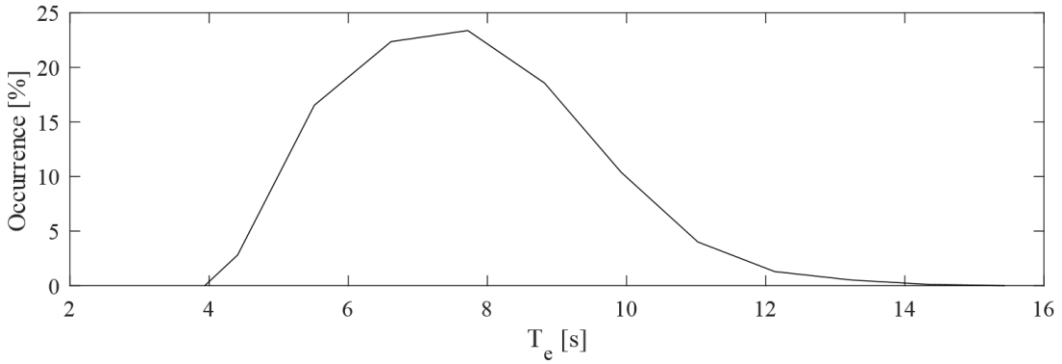

Figure 11. Occurrence of energy period T_e for Belmullet in Ireland

The annual energy yield, E_S, for each sea state is computed as:

$$E_S = P_{av}(S)p(S)8760 \tag{8}$$

where $P_{av}(S)$ is time-averaged power output from the device for sea-state *S*, $p(S)$ is the probability of occurrence for the sea-state, and 8760 is the number of hours in a typical year. The total annual energy yield is the sum of the annual energy yield for each sea-state, $E = \sum E_S$, and the average power from the site is $P_{av} = \frac{E}{8760}$. Finally, the rated power in this work is assumed to be three times the average power, i.e. $P_{rated} = 3P_{av}$, in accordance with [3].

Capture width (CW) is a parameter that characterises the performance of a WEC. It is the width of the wave front (assuming unidirectional waves) that contains the same amount of power as that absorbed by the WEC [28]. CW is defined as the ratio of the absorbed power, $P_{av}(S)$, to the power in a unit width wave front, P_w. In order to describe the efficiency of a WEC in practical situations capture width ratio (CWR) is usually introduced. CWR is sometimes normalised by body width but this does not generalise performance and hence does not enable device comparison [3]. In this work CWR is normalised by the wavelength $L_e = \frac{gT_e{}^2}{2\pi}$ associated with peak energy period:

$$CWR = \frac{\left(\frac{P_{av}(S)}{P_w}\right)}{L_e} \tag{9}$$

The power in a unit width wave front is calculated based on linear theory where:

$P_w =$ Power in a unit width wave front , $P_w = \frac{1}{2}\rho g \xi_A^2 c_g$,

$c_g = group\ velocity, c_g = \frac{c_w}{2}\left(1 + \frac{2kh}{\sinh(2kh)}\right)$,

$c_w = wave\ celerity, c_w = \frac{\omega}{k}$,

$k = wave\ number, k = \frac{\omega^2}{g \cdot \tanh(kh)}$.

In [3], the root-mean-square error (RMSE) of the angle between the floats, θ_{rms} is presented, which gives a measure of relative pitching between the floats in each sea-state. It is also calculated in this work between the bow and stern floats using eqn. (10) in order to validate the MFM for several sea states observed over time *T*.

$$\theta_{rms} = \sqrt{\frac{\sum_t^T \left(\omega^{(1)}(t) - \omega^{(3)}(t)\right)}{T}} \tag{10}$$

The same method is used to find the RMSE of time-series results from the MFM model compared to the vectorial mechanics model from [3] to give a quantitative measure of the discrepancy. Eqn. (11) measures the average difference between two time series $X_1(t)$ and $X_2(t)$:

$$RMSE = \sqrt{\frac{\sum_t^T \left(X_1(t) - X_2(t)\right)}{T}} \tag{11}$$

The following sections introduce and summarise the MFM before commencing an analysis of the three-float M4 WEC in irregular sea-states.

3 THE MOVING FRAME METHOD

The MFM is based upon modern mathematical tools developed during the last century.

Élie Cartan (1869-1951) [29] assigned a reference frame to each point of an object under study (a curve, a surface, the Euclidean space itself). Using an orthonormal expansion, he expressed the rate of change of the frame in terms of the frame. The MFM adopts this concept by placing a reference frame on every moving link. Following, a method is needed to express the relationships between frames. For this, the focus is shifted to the work of Sophus Lie.

Marius Sophus Lie (1842-1899) [30] developed the theory of continuous groups and their associated algebras. The MFM adopts the mathematics of rotation groups and their algebras yet distils them to simple matrix multiplications. However, a simplifying notation is needed. For this, the focus is shifted to Frankel.

Theodore Frankel (1929-2017) [31] developed a compact notation in geometrical physics. The MFM adopts this notation to enable a methodology that is identical for both 2D and 3D analyses. The notation is identical for single and multi-body linked systems.

The MFM replaces an inordinate reliance on vector algebra with the framework of Lie algebra reduced to the simplicity of rotation matrices. It abandons the inertial frame in favour of the moving frame as a formative element. An introduction to the Moving Frame Method (for single rigid bodies) along with a pedagogical assessment is available in *The moving frame method in dynamics: Reforming a curriculum and assessment* by Impelluso [32]. The following sections summarise the MFM.

3.1 Single Body Kinematics Using SO(3)

At the center of mass of each moving body (α) a time-dependent (moving) frame is attached:

$$\mathbf{e}^{(\alpha)}(t) = \left(\mathbf{e}_1^{(\alpha)}(t)\ \ \mathbf{e}_2^{(\alpha)}(t)\ \ \mathbf{e}_3^{(\alpha)}(t)\right) \tag{12}$$

In eqn. (12), each $\mathbf{e}_i^{(\alpha)}(t)$ is a unit vector, where the subscript denotes the direction.

An inertial frame is defined at $t = 0$ and deposited from any specified moving frame:

$$\mathbf{e}^I = \left(\mathbf{e}_1^I\ \ \mathbf{e}_2^I\ \ \mathbf{e}_3^I\right) = \left(\mathbf{e}_1^{(\alpha)}(0)\ \ \mathbf{e}_2^{(\alpha)}(0)\ \ \mathbf{e}_3^{(\alpha)}(0)\right) \tag{13}$$

The point-wise principle assures that if such a frame is deposited anywhere, and is inertial, it can be considered as a reference inertial frame. Figure 12 visualises a fixed inertial frame deposited at $t = 0$ and a moving frame that has translated relative to the inertial frame.

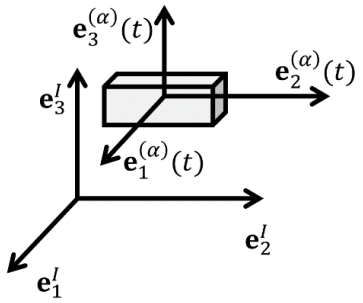

Figure 12. Inertial frame, $\boldsymbol{e}^I$, and translated moving frame, $\boldsymbol{e}^{(\alpha)}$

The absolute position vector $\mathbf{r}^{(\alpha)}(t)$ of this moving frame is defined as a translation from the inertial frame $\mathbf{e}^I$:

$$\mathbf{r}^{(\alpha)}(t) = \mathbf{e}^I x^{(\alpha)}(t) \tag{14}$$

Above, $x^{(\alpha)}(t)$ represents the *absolute* coordinates of the distance from the inertial frame to the center of mass of a body, expressed in the inertial frame. However, using bold $\boldsymbol{s}$ for the vector and non-bold s for the components, the *relative* position vector of a moving frame ($\alpha + 1$) from another moving frame (α) is asserted as:

$$\mathbf{s}^{(\alpha+1/\alpha)}(t) = \mathbf{e}^{(\alpha)}(t) s^{(\alpha+1/\alpha)}(t) \tag{15}$$

Next, the absolute position vector of the α-frame, $\mathbf{r}^{(\alpha)}(t)$, and the relative position vector $\mathbf{s}^{(\alpha+1/\alpha)}(t)$ are combined to obtain the absolute position vector of the (α + 1) frame:

$$\mathbf{r}^{(\alpha+1)}(t) = \mathbf{r}^{(\alpha)}(t) + \mathbf{e}^{(\alpha)}(t) s^{(\alpha+1/\alpha)}(t) \tag{16}$$

This is visualised for frames $\mathbf{e}^{(1)}(t)$ and $\mathbf{e}^{(2)}(t)$ in Figure 13 below:

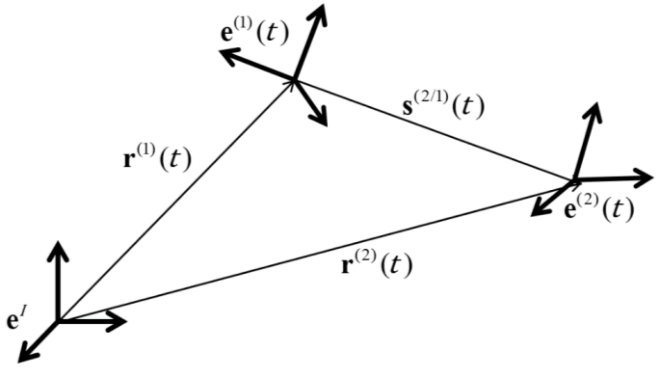

Figure 13. Relationships between relative, **r**, and absolute, **s**, position vectors

The attention is turned to frame orientations. A rotation matrix, $R^{(\alpha)}(t)$, a member of the Special Orthogonal Group (SO(3)), relates the orientation of a moving frame from an inertial frame:

$$\mathbf{e}^{(\alpha)}(t) = \mathbf{e}^{I} R^{(\alpha)}(t) \tag{17}$$

Figure 14 visualises a fixed inertial frame deposited at t = 0 and a moving frame that has rotated relative to the inertial frame:

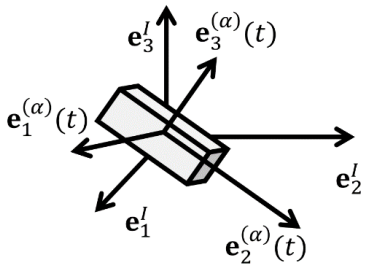

Figure 14. Inertial frame, $\boldsymbol{e}^{I}$, and rotated moving frame, $\boldsymbol{e}^{(\alpha)}$

The relative rotation of a frame (α + 1) from another frame (α) is designated as:

$$\mathbf{e}^{(\alpha+1)}(t) = \mathbf{e}^{(\alpha)}(t) R^{(\alpha+1/\alpha)}(t) \tag{18}$$

The orientation of body ($\alpha + 1$) from the inertial frame is found by inserting eqn. (17) into (18) and exploiting the closure property of the SO(3) Group:

$$\mathbf{e}^{(\alpha+1)}(t) = \mathbf{e}^{I} R^{(\alpha)}(t) R^{(\alpha+1/\alpha)}(t) = \mathbf{e}^{I}\, R^{(\alpha+1)}(t) \tag{19}$$

One defining property of SO(3) is that the inverse of a rotation matrix is the transpose of the rotation matrix:

$$\left(R^{(\alpha)}(t)\right)^{-1} = \left(R^{(\alpha)}(t)\right)^{T} \tag{20}$$

Keeping in mind that the inertial frame remains constant, the time rate of frame rotation is found as:

$$\dot{\mathbf{e}}^{(\alpha)}(t) = \mathbf{e}^{I} \dot{R}^{(\alpha)}(t) \tag{21}$$

Noting that $\left(R^{(\alpha)}(t)\right)^{-1}\left(R^{(\alpha)}(t)\right)$ is equal to an identity matrix, eqn. (20) is used in eqn. (17) to formulate the inertial frame in terms of the moving frame:

$$\mathbf{e}^{I} = \mathbf{e}^{(\alpha)}(t)\left(R^{(\alpha)}(t)\right)^{T} \tag{22}$$

This is substituted back into eqn. (21) to obtain the time rate of frame rotation expressed in its own frame:

$$\dot{\mathbf{e}}^{(\alpha)}(t) = \mathbf{e}^{(\alpha)}(t)\left(R^{(\alpha)}(t)\right)^{T} \dot{R}^{(\alpha)}(t) \tag{23}$$

The associated algebra, so(3), of the SO(3) group, affirms that the matrix product in eqn. (23) is skew-symmetric (all dominant diagonal terms are zero). The skew-symmetric angular velocity, $\overleftrightarrow{\omega^{(\alpha)}(t)}$, is defined in eqn. (24):

$$\overleftrightarrow{\omega^{(\alpha)}(t)} = \left(R^{(\alpha)}(t)\right)^T \dot{R}^{(\alpha)}(t) = \begin{bmatrix} 0 & -\omega_3^{(\alpha)}(t) & \omega_2^{(\alpha)}(t) \\ \omega_3^{(\alpha)}(t) & 0 & -\omega_1^{(\alpha)}(t) \\ -\omega_2^{(\alpha)}(t) & \omega_1^{(\alpha)}(t) & 0 \end{bmatrix} \tag{24}$$

Eqn. (23) is rewritten as:

$$\dot{\mathbf{e}}^{(\alpha)}(t) = \mathbf{e}^{(\alpha)}(t)\overleftrightarrow{\omega^{(\alpha)}(t)} \tag{25}$$

The components of the skew-symmetric angular velocity are isomorphic to the components of an angular velocity vector, $\boldsymbol{\omega}^{(\alpha)}(t)$, when associated with the same frame as was used in its construction. This column is associated with the same frame in which the relationships were derived.

$$\boldsymbol{\omega}^{(\alpha)}(t) = \mathbf{e}^{(\alpha)}(t)\begin{pmatrix} \omega_1^{(\alpha)}(t) \\ \omega_2^{(\alpha)}(t) \\ \omega_3^{(\alpha)}(t) \end{pmatrix} \tag{26}$$

3.2 Structured Kinematics Using SE(3)

This analysis can be completed using free body diagrams and elements of the Special Orthogonal Group. However, this section introduces the Special Euclidean Group (SE(3)) to accelerate the analysis of the kinetics of multi-body systems in 3D.

The aim of SE(3) is to combine the rotational and translational data of a frame α into one structure. To accomplish this, the 4×4 absolute *frame connection matrix* (a member of the Special Euclidean Group), E, is defined. It is essential to note that $E \in$ SE(3), while $R \in$ SO(3).

$$E^{(\alpha)}(t) = \begin{bmatrix} R^{(\alpha)}(t) & x^{(\alpha)}(t) \\ 0_3^T & 1 \end{bmatrix} \tag{27}$$

Next, a moving frame and its location from an inertial frame are combined in one data structure. This is defined as a *moving frame connection*:

$$\left(\mathbf{e}^{(\alpha)}(t)\,\mathbf{r}^{(\alpha)}(t)\right)=\left(\mathbf{e}_1^{(\alpha)}(t)\;\;\mathbf{e}_2^{(\alpha)}(t)\;\;\mathbf{e}_3^{(\alpha)}(t)\;\;\mathbf{r}^{(\alpha)}(t)\right) \tag{28}$$

Similarly, if the frame is inertial, the data structure consists of an inertial frame and the location to the inertial frame, which is always zero. This is defined as the *inertial frame connection*:

$$\left(\mathbf{e}^{I}\;\mathbf{0}\right)=\left(\mathbf{e}_1^{I}\;\;\mathbf{e}_2^{I}\;\;\mathbf{e}_3^{I}\;\mathbf{0}\right) \tag{29}$$

The inertial frame connection (eqn. (29)) and the moving frame connection (eqn. (28)) are related by utilising the absolute frame connection matrix (eqn. (27)):

$$\left(\mathbf{e}^{(\alpha)}(t)\,\mathbf{r}^{(\alpha)}(t)\right)=(\mathbf{e}^{I}\;\mathbf{0})E^{(\alpha)}(t) \tag{30}$$

The compact form of the absolute frame connection matrix is written as:

$$\left(\mathbf{e}^{(\alpha)}(t)\,\mathbf{r}^{(\alpha)}(t)\right)=(\mathbf{e}^{I}\;\mathbf{0})\begin{bmatrix} R^{(\alpha)}(t) & x^{(\alpha)}(t) \\ 0_3^T & 1 \end{bmatrix} \tag{31}$$

Multiplying out gives the same relations as for SO(3) as seen in eqns. (14) and (17):

$$\left(\mathbf{e}^{(\alpha)}(t)\,\mathbf{r}^{(\alpha)}(t)\right)=(\mathbf{e}^{I}R^{(\alpha)}(t)\;\;\mathbf{e}^{I}x^{(\alpha)}(t)) \tag{32}$$

Likewise, the *relative* frame connection matrix consists of the relative rotation matrix and the relative position vector and is defined as:

$$E^{(\alpha+1/\alpha)}(t)=\begin{bmatrix} R^{(\alpha+1/\alpha)}(t) & s^{(\alpha+1/\alpha)}(t) \\ 0_3^T & 1 \end{bmatrix} \tag{33}$$

Eqn. (33) is used to express the relationship between two moving frames, (α+1) and α:

$$\left(\mathbf{e}^{(\alpha+1)}(t)\,\mathbf{r}^{(\alpha+1)}(t)\right)=\left(\mathbf{e}^{(\alpha)}(t)\,\mathbf{r}^{(\alpha)}(t)\;\right)E^{(\alpha+1/\alpha)}(t) \tag{34}$$

Again, eqn. (34), with its defining element (eqn. (33)), recapitulates eqns. (16) and (18).

Next, the *absolute* frame connection matrix of body (α+1) is found. This is the product of the absolute frame connection matrix of body (α) and the relative frame connection matrix of (α+1) from (α):

$$E^{(\alpha+1)}(t) = E^{(\alpha)}(t)E^{(\alpha+1/\alpha)}(t) \tag{35}$$

The inverse of the frame connection matrix is known analytically (due to $E \in$ SE(3)) and expressed as:

$$\left(E^{(\alpha)}(t)\right)^{-1} = \begin{bmatrix} \left(R^{(\alpha)}(t)\right)^T & -\left(R^{(\alpha)}(t)\right)^T x^{(\alpha)}(t) \\ 0_3^T & 1 \end{bmatrix} \tag{36}$$

Eqn. (36) is used in eqn. (30) to formulate the inertial frame connection in terms of the moving frame connection:

$$\left(\mathbf{e}^I \;\; \mathbf{0}\right) = \left(\mathbf{e}^{(\alpha)}(t) \;\; \mathbf{r}^{(\alpha)}(t)\right)\left(E^{(\alpha)}(t)\right)^{-1} \tag{37}$$

This result along with the time rate of eqn. (30) is used to obtain the time rate of the frame connection in terms of the frame connection itself:

$$\left(\dot{\mathbf{e}}^{(\alpha)}(t) \;\; \dot{\mathbf{r}}^{(\alpha)}(t)\right) = \left(\mathbf{e}^{(\alpha)}(t) \;\; \mathbf{r}^{(\alpha)}(t)\right)\left(E^{(\alpha)}(t)\right)^{-1} \dot{E}^{(\alpha)}(t) \tag{38}$$

The absolute time rate of frame connection matrix for the body, $\Omega^{(\alpha)}$, is defined as the product of $\left(E^{(\alpha)}(t)\right)^{-1}$ and $\dot{E}^{(\alpha)}(t)$. Eqn. (38) is rewritten as:

$$\left(\dot{\mathbf{e}}^{(\alpha)}(t) \;\; \dot{\mathbf{r}}^{(\alpha)}(t)\right) = \left(\mathbf{e}^{(\alpha)}(t) \;\; \mathbf{r}^{(\alpha)}(t)\right)\Omega^{(\alpha)}(t) \tag{39}$$

$\Omega^{(\alpha)}$ presented in matrix form is:

$$\Omega^{(\alpha)} = \begin{bmatrix} \overrightarrow{\omega^{(\alpha)}(t)} & \left(R^{(\alpha)}(t)\right)^T \dot{x}^{(\alpha)}(t) \\ 0_3^T & 0 \end{bmatrix} \tag{40}$$

4 DYNAMICS OF THE M4 WAVE ENERGY CONVERTER

Before continuing with the SE(3) aspects of the MFM, inertial parameters are presented. The bow float is defined as float 1, mid float as float 2 and stern float as float 3. The horizontal and vertical distance from float 1 centre of mass (yellow dot at float 1) to float 2 centre of mass (yellow dot at float 2) is defined as $s_1^{(2/1)}$ and $s_3^{(2/1)}$ respectively. The vertical distance from float 2 to the hinge is defined as $s^{(h/2)}$ and the horizontal and vertical distance from the hinge to float 3 centre of mass (yellow dot at float 3) is defined as $s_1^{(3/h)}$ and $s_3^{(3/h)}$, respectively. These variables are used later when constructing the equations of motion with the moving frame method and are seen in Figure 15:

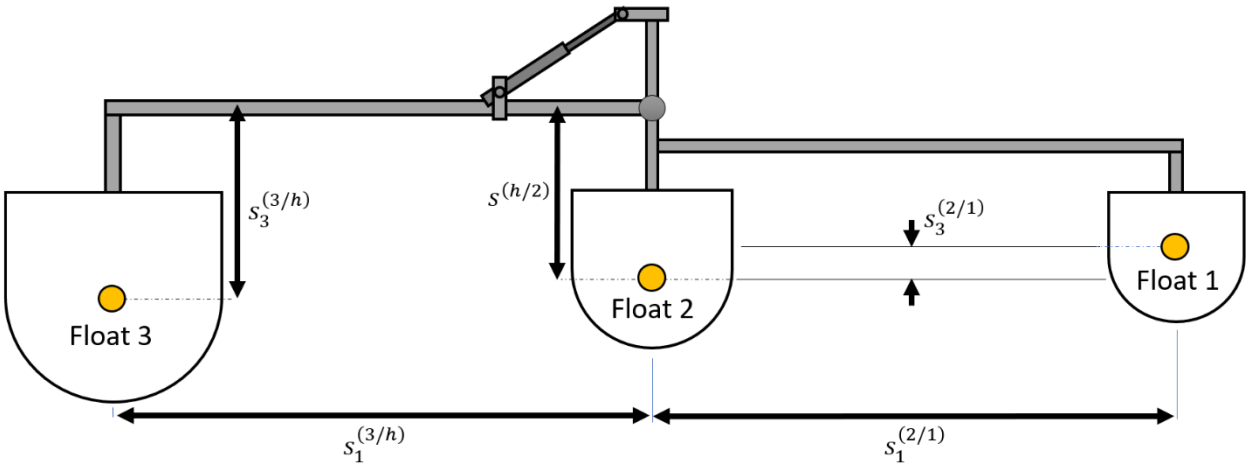

Figure 15. Schematic of M4 WEC relative distances between each floats' center of mass (●).

Distances (as seen in Figure 9) and masses for the floats have been established in prior research [3] and are presented in Table 2.

4.1 Moment of Inertia

The moving frame method relies on finding the mass moment of inertia, which is a rotating body's resistance to angular acceleration, about the centre of mass of each body in a multi-link system. This thesis uses the established moment of inertias from previous work [3], however the moments of inertia from [3] is established about a distal hinge. Thus, it is incumbent to first transition the mass moment of inertia from that pre-established hinge, back to the centre of mass of the individual components, and finally reconstruct mass moment of inertia about each floats' centre of mass.

The parallel axis theorem is used to find the 3D mass moment of inertia about the centre of mass of the floats. In eqn. (41), d is the coordinates of the centre of mass from some arbitrary point O. J_C is the moment of inertia when the frame is at the centre of mass and J_O is the moment of inertia when the frame is at some arbitrary point, O.

$$J_O = m\overleftrightarrow{d}\,\overleftrightarrow{d}^T + J_C = m\begin{bmatrix} 0 & -d_3 & d_2 \\ d_3 & 0 & -d_1 \\ -d_2 & d_1 & 0 \end{bmatrix}\begin{bmatrix} 0 & d_3 & -d_2 \\ -d_3 & 0 & d_1 \\ d_2 & -d_1 & 0 \end{bmatrix} + J_C \tag{41}$$

The moment of inertia about the centre of mass of each float, in addition to the distances and masses, are presented in Table 2:

Table 2. Mass, moment of inertia and distances for each float

Body	**Unit**	**Symbol**	
Float 1 (bow float)	Mass [kg]	$m^{(1)}$	2.2
	Inertia [kgm^2]	$J_2^{(1)}$	0.204
	Distance [m]	$s^{(2/1)}$	$\begin{bmatrix} 1.330 \\ 0 \\ 0.01 \end{bmatrix}$
Float 2 (mid float)	Mass [kg]	$m^{(2)}$	4.887
	Inertia [kgm^2]	$J_2^{(2)}$	0.075
	Distance [m]	$s^{(h/2)}$	$\begin{bmatrix} 0 \\ 0 \\ 0.283 \end{bmatrix}$
Float 3 (stern float)	Mass [kg]	$m^{(3)}$	17.24
	Inertia [kgm^2]	$J_2^{(3)}$	0.614
	Distance [m]	$s^{(3/h)}$	$\begin{bmatrix} 0.8 \\ 0 \\ 0.333 \end{bmatrix}$

4.2 First Frame – Float 1

Figure 16 illustrates the wave energy converter with moving frames positioned at the centre of mass of their associated bodies, where the superscript indicates which float the frame is positioned at, and the subscript indicates direction. The direction vectors are aligned with the typical XYZ orientations of marine bodies such that later comparison with diffraction coefficients, obtained from a panel code, WaveAnalysisMIT (WAMIT), is maintained.

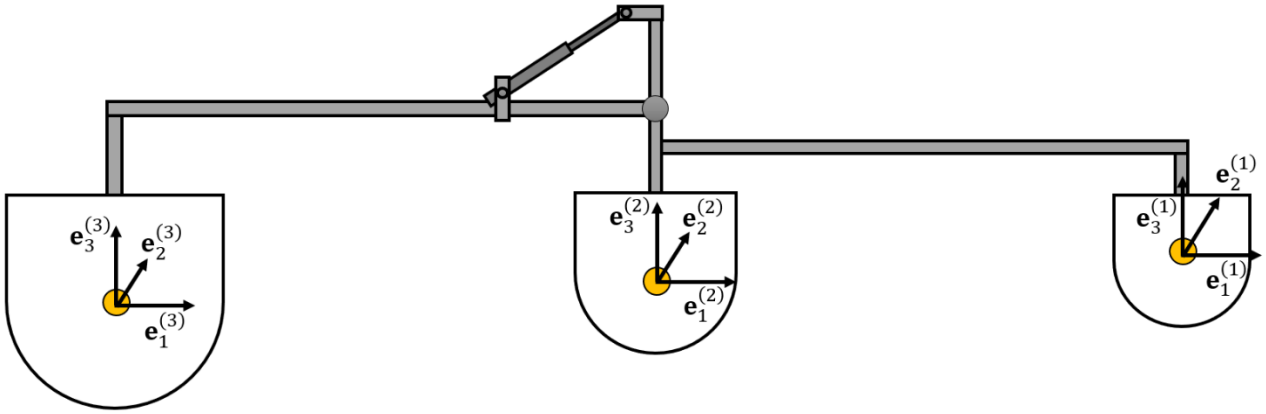

Figure 16. Diagram of the three-float M4 device with frames

At $t = 0$ an inertial frame is deposited from the first frame:

$$\mathbf{e}^{I} = \mathbf{e}^{(1)}(0) \tag{42}$$

Although the inertial frame is deposited from the first frame, it remains and serves as the inertial frame for the position data of the entire system. Next, a frame connection matrix is defined for the first frame:

$$E^{(1)}(t) = \begin{bmatrix} R^{(1)}(t) & x^{(1)}(t) \\ 0_3^T & 1 \end{bmatrix} \tag{43}$$

$R^{(1)}(t)$ represents the rotation of the first float and has the general form:

$$R^{(1)}(t) \equiv \begin{bmatrix} R_{11}^{(1)}(t) & R_{12}^{(1)}(t) & R_{13}^{(1)}(t) \\ R_{21}^{(1)}(t) & R_{22}^{(1)}(t) & R_{23}^{(1)}(t) \\ R_{31}^{(1)}(t) & R_{32}^{(1)}(t) & R_{33}^{(1)}(t) \end{bmatrix} \tag{44}$$

$x^{(1)}(t)$ represents the possible translation of the first float. Eqns. (27-40) are used to find the absolute time rate of frame connection matrix for the first float:

$$\Omega^{(1)} = \begin{bmatrix} \overleftrightarrow{\omega^{(1)}(t)} & \left(R^{(1)}(t)\right)^T \dot{x}^{(1)}(t) \\ 0_3^T & 0 \end{bmatrix} \tag{45}$$

From eqn. (45), the time rate of the first frame is extracted:

$$\dot{\mathbf{e}}^{(1)}(t) = \mathbf{e}^{(1)}(t)\overleftrightarrow{\omega^{(1)}(t)} \tag{46}$$

The second equation is also extracted:

$$\dot{\mathbf{r}}^{(1)}(t) = \mathbf{e}^{(1)}(t)\left(R^{(1)}(t)\right)^T \dot{x}^{(1)}(t) \tag{47}$$

The translational velocity of the first frame is asserted as:

$$\dot{\mathbf{r}}^{(1)}(t) = \mathbf{e}^I \dot{x}^{(1)}(t) \tag{48}$$

4.3 Second Frame – Float 2

At the centre of mass of float 2, a moving frame $\mathbf{e}^{(2)}$(t) is positioned. In keeping with the analysis of multi-body systems, the next task is to "locate" the second frame from the first frame. However, due to the rigid connection between float 1 and float 2, the two floats move together. One solution is to define float 1 and float 2 as one single body – but this complicates the equations when it comes to computing forces and moments induced by waves. A better solution is to place a moving frame at the centre of mass of float 2 and lock it with the same rotational orientation as float 1. Thus, in order to locate the second frame from the first frame, the first frame is simply parallel translated with no rotation. This fixed path is illustrated in Figure 17 below (dotted red line) and the distance,

$s^{(2/1)}$, is presented in Table 2. Henceforth, float 1 orientation is determined by forces and moments induced by waves acting on both floats 1 and 2, and the orientation of float 2 is found from the orientation of float 1.

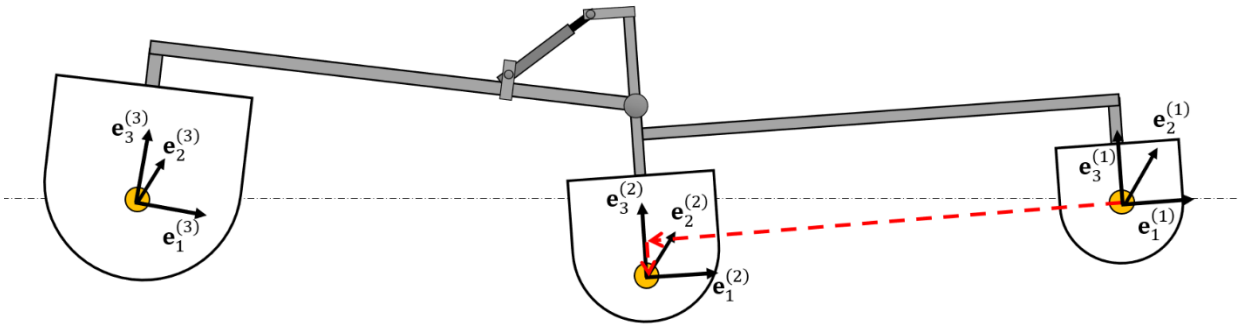

Figure 17. Fixed path from float 1 to float 2 (compressed actuator)

A common practise is to rotate frame 1 in order to obtain the orientation of frame 2. However, this work demonstrates that a moving frame that is unable to rotate is very useful for obtaining the accurate forces and their associated moments. The rotation matrix from frame 2 to frame 1 is therefore identical to the identity matrix.

$$\mathbf{e}^{(2)}(t) = \mathbf{e}^{(1)}(t)R^{(2/1)}(t) = \mathbf{e}^{(1)}(t)\begin{bmatrix} 1 & 0 & 0 \\ 0 & 1 & 0 \\ 0 & 0 & 1 \end{bmatrix} \tag{49}$$

This information is used to construct the relative frame connection matrix:

$$E^{(2/1)}(t) = \begin{bmatrix} I_3 & s^{(2/1)} \\ 0_3^T & 1 \end{bmatrix} \tag{50}$$

Using eqn. (35), the absolute frame connection matrix $E^{(2)}$(t) is found:

$$E^{(2)}(t) = \begin{bmatrix} R^{(1)}(t) & R^{(1)}(t)s^{(2/1)} + x^{(1)}(t) \\ 0_3^T & 1 \end{bmatrix} \tag{51}$$

Finally, the time rate of the frame connection of the second frame is:

$$\left(\dot{\mathbf{e}}^{(2)}(t)\ \ \dot{\mathbf{r}}^{(2)}(t)\right)=\left(\mathbf{e}^{(2)}(t)\ \ \mathbf{r}^{(2)}(t)\right)\left(E^{(2)}(t)\right)^{-1}\dot{E}^{(2)}(t)=\left(\mathbf{e}^{(2)}(t)\ \ \mathbf{r}^{(2)}(t)\right)\Omega^{(2)}(t) \tag{52}$$

In its full form, the absolute time rate of frame connection matrix is:

$$\Omega^{(2)}(t)=\begin{bmatrix}\left(R^{(1)}(t)\right)^{T}\dot{R}^{(1)}(t) & \left(R^{(1)}(t)\right)^{T}\left(\dot{R}^{(1)}(t)s^{(2/1)}+\dot{x}^{(1)}(t)\right)\\ 0_3^T & 0\end{bmatrix} \tag{53}$$

From eqn. (53), the angular velocity vectors and linear velocity vectors of the second frame are extracted. Eqns. (17) and (18) are used to find the linear velocity vector of the second frame with respect to the inertial frame:

$$\boldsymbol{\omega}^{(2)}(t)=\mathbf{e}^{(2)}(t)\left(\omega^{(1)}(t)\right) \tag{54}$$

$$\dot{\mathbf{r}}^{(2)}(t)=\mathbf{e}^{I}\left\{R^{(1)}(t)\overleftrightarrow{s^{(2/1)}}^{T}\omega^{(1)}(t)+\dot{x}^{(1)}(t)\right\} \tag{55}$$

As expected, the angular velocity of the second frame is indistinguishable to the angular velocity of the first frame. Next, the same procedure is followed in order to find the angular- and linear velocity vector for the final moving frame.

4.4 Third Frame – Float 3

At the centre of mass of float 3, a moving frame $\mathbf{e}^{(3)}(t)$ is positioned. The next task is to "locate" the third frame from the second frame. First, the second frame is parallel translated to the hinge (follow the red line in Figure 18); then the frame is rotated with respect to $\mathbf{e}_2$; finally, the frame is parallel translated to the third floats centre of mass (follow the green line in Figure 18).

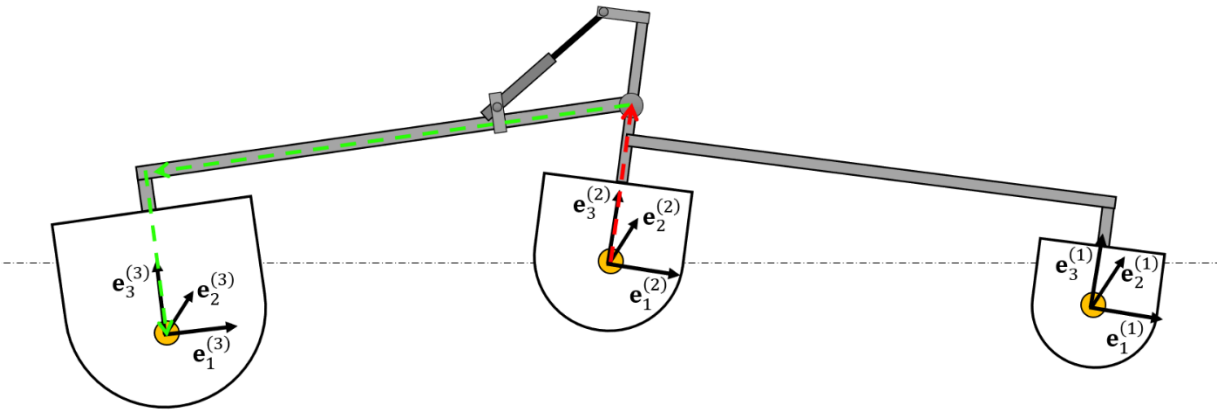

Figure 18. Fixed path from float 2 to float 3 (extended actuator)

The distance from float 2 to the hinge, $s^{(h/2)}$, and the distance from the hinge to float 3, $s^{(3/h)}$, are presented in Table 2. With specific regard to the hinge, the orientation of the third frame is obtained from the second frame by rotating $\varphi^{(3/2)}$(t) about the common 2-axis:

$$\mathbf{e}^{(3)}(t) = \mathbf{e}^{(2)}(t)R^{(3/2)}(t) = \mathbf{e}^{(2)}(t)\begin{bmatrix} \cos\varphi^{(3/2)}(t) & 0 & \sin\varphi^{(3/2)}(t) \\ 0 & 1 & 0 \\ -\sin\varphi^{(3/2)}(t) & 0 & \cos\varphi^{(3/2)}(t) \end{bmatrix} \tag{56}$$

This information is used to construct the relative frame connection matrix:

$$E^{(3/2)}(t) = \begin{bmatrix} I_3 & s^{(h/2)} \\ 0_3^T & 1 \end{bmatrix}\begin{bmatrix} R^{(3/2)}(t) & 0_3 \\ 0_3^T & 1 \end{bmatrix}\begin{bmatrix} I_3 & s^{(3/h)} \\ 0_3^T & 1 \end{bmatrix} \tag{57}$$

The following expression for the relative frame connection matrix is obtained:

$$E^{(3/2)}(t) = \begin{bmatrix} R^{(3/2)}(t) & R^{(3/2)}(t)s^{(3/h)} + s^{(h/2)} \\ 0_3^T & 1 \end{bmatrix} \tag{58}$$

Using eqn. (35) the absolute frame connection matrix $E^{(3)}$(t) is found:

$$E^{(3)}(t) = \begin{bmatrix} R^{(1)}(t)R^{(3/2)}(t) & R^{(1)}(t)\left(R^{(3/2)}(t)s^{(3/h)} + s^{(h/2)}\right) + \left\{R^{(1)}(t)s^{(2/1)} + x^{(1)}(t)\right\} \\ 0_3^T & 1 \end{bmatrix} \tag{59}$$

Finally, the time rate of the frame connection of the third float is:

$$\left(\dot{\mathbf{e}}^{(3)}(t)\ \ \dot{\mathbf{r}}^{(3)}(t)\right)=\left(\mathbf{e}^{(3)}(t)\ \ \mathbf{r}^{(3)}(t)\right)\left(E^{(3)}(t)\right)^{-1}\dot{E}^{(3)}(t)=\left(\mathbf{e}^{(3)}(t)\ \ \mathbf{r}^{(3)}(t)\right)\Omega^{(3)}(t) \tag{60}$$

From eqn. (60) the angular velocity vectors and linear velocity vectors of the third frame are obtained:

$$\boldsymbol{\omega}^{(3)}(t)=\mathbf{e}^{(3)}(t)\left(\left(R^{(3/2)}(t)\right)^{T}\omega^{(1)}(t)+\omega^{(3/2)}(t)\right) \tag{61}$$

$$\dot{\mathbf{r}}^{(3)}(t)=\mathbf{e}^{I}\left(R^{(1)}(t)R^{(3/2)}(t)\overleftrightarrow{s^{(3/h)}}^{T}\omega^{(3)}(t)+R^{(1)}(t)\overleftrightarrow{s^{(h/2)}}^{T}\omega^{(1)}(t)+\dot{x}^{(2)}(t)\right) \tag{62}$$

4.5 Simplifications and Generalised Coordinates

Before continuing, all the required equations are summarised; linear- and angular velocity of float 1 to 3, respectively.

First, the linear and angular velocity of float 1:

$$\dot{x}^{(1)}(t)=\begin{pmatrix}\dot{x}_1^{(1)}(t)\\ \dot{x}_2^{(1)}(t)\\ \dot{x}_3^{(1)}(t)\end{pmatrix} \tag{63}$$

$$\omega^{(1)}(t)=\begin{pmatrix}\omega_1^{(1)}(t)\\ \omega_2^{(1)}(t)\\ \omega_3^{(1)}(t)\end{pmatrix} \tag{64}$$

Next, the linear and angular velocity of float 2:

$$\dot{x}^{(2)}(t)=R^{(1)}(t)\overleftrightarrow{s^{(2/1)}}^{T}\omega^{(1)}(t)+\dot{x}^{(1)}(t) \tag{65}$$

$$\omega^{(2)}(t)=\omega^{(1)}(t) \tag{66}$$

Finally, the linear and angular velocity of float 3:

$$\dot{x}^{(3)}(t) = R^{(1)}(t)R^{(3/2)}(t)\overleftarrow{s^{(3/h)}}^{T}\omega^{(3)}(t) + R^{(1)}(t)\overleftarrow{s^{(h/2)}}^{T}\omega^{(1)}(t) + \dot{x}^{(2)}(t) \tag{67}$$

$$\omega^{(3)}(t) = \left(R^{(3/2)}(t)\right)^{T}\omega^{(1)}(t) + \omega^{(3/2)}(t) \tag{68}$$

Some kinematic assumptions are made before proceeding with finding and solving the differential equations. One major advantage for including these assumptions in the analysis is that the results are comparable to an experimentally-validated vectorial mechanics model from [3]. The results will confirm if hydrodynamic forces in an irregular sea-state have been successfully implemented into the MFM.

Rotational and angular velocity simplifications

Prior research reveals that roll is eliminated by adding out-rigger buoys to the stern float [3]; so, roll motion is ignored. Another assumption is to ignore yawing since this does not affect the resultant power output significantly. With these assumptions, the full rotation matrix of the first float greatly simplifies:

$$R^{(1)}(t) = \begin{bmatrix} R_{11}^{(1)}(t) & R_{12}^{(1)}(t) & R_{13}^{(1)}(t) \\ R_{21}^{(1)}(t) & R_{22}^{(1)}(t) & R_{23}^{(1)}(t) \\ R_{31}^{(1)}(t) & R_{32}^{(1)}(t) & R_{33}^{(1)}(t) \end{bmatrix} \xrightarrow{No\ roll\ /\ yaw} \begin{bmatrix} \cos\theta^{(1)}(t) & 0 & \sin\theta^{(1)}(t) \\ 0 & 1 & 0 \\ -\sin\theta^{(1)}(t) & 0 & \cos\theta^{(1)}(t) \end{bmatrix} \tag{69}$$

Furthermore, these assumptions also simplify the angular velocity of the first float:

$$\omega^{(1)}(t) = \begin{pmatrix} \omega_1^{(1)}(t) \\ \omega_2^{(1)}(t) \\ \omega_3^{(1)}(t) \end{pmatrix} \xrightarrow{No\ roll\ /\ yaw} \begin{pmatrix} 0 \\ \dot{\theta}^{(1)}(t) \\ 0 \end{pmatrix} \tag{70}$$

Translational simplifications

The M4 wave energy converter is assumed to only translate in surge and heave. Translation in sway is not of great importance when investigating the power output since the PTO cannot absorb power in this direction. This simplifies the linear velocity for the first float (and consequently also simplifies linear velocity for the second and third float):

$$\dot{x}^{(1)}(t) = \begin{pmatrix} \dot{x}_1^{(1)}(t) \\ \dot{x}_2^{(1)}(t) \\ \dot{x}_3^{(1)}(t) \end{pmatrix} \xrightarrow{No\ sway} \begin{pmatrix} \dot{x}_1^{(1)}(t) \\ 0 \\ \dot{x}_3^{(1)}(t) \end{pmatrix} \tag{71}$$

The next step is to define a minimal set of generalised coordinates.

Generalised coordinates

The full list of *Cartesian velocities* is denoted as $\{\dot{X}(t)\}$. This column vector contains three linear- and angular velocity components for each float and is 18x1 in size. A minimal set of *generalised velocities* needed to model the configuration of the system is deployed and is denoted as $\{\dot{q}(t)\}$. The generalised velocities consist of surge, heave and pitch velocity of the bow float, and the pitch velocity of the stern float relative to the mid float and is 4x1 in size. In other words, all 18 Cartesian velocities are computed from the minimal set of generalised velocities. Eqn. (72) shows the full list of Cartesian and generalised velocities:

$$\left\{\dot{X}(t)\right\} \equiv \begin{pmatrix} \dot{x}_1^{(1)}(t) \\ \dot{x}_2^{(1)}(t) \\ \dot{x}_3^{(1)}(t) \\ \omega_1^{(1)}(t) \\ \omega_2^{(1)}(t) \\ \omega_3^{(1)}(t) \\ \dot{x}_1^{(2)}(t) \\ \dot{x}_2^{(2)}(t) \\ \dot{x}_3^{(2)}(t) \\ \omega_1^{(2)}(t) \\ \omega_2^{(2)}(t) \\ \omega_3^{(2)}(t) \\ \dot{x}_1^{(3)}(t) \\ \dot{x}_2^{(3)}(t) \\ \dot{x}_3^{(3)}(t) \\ \omega_1^{(3)}(t) \\ \omega_2^{(3)}(t) \\ \omega_3^{(3)}(t) \end{pmatrix} \equiv \begin{pmatrix} \dot{x}^{(1)}(t) \\ \omega^{(1)}(t) \\ \dot{x}^{(2)}(t) \\ \omega^{(2)}(t) \\ \dot{x}^{(3)}(t) \\ \omega^{(3)}(t) \end{pmatrix}, \quad \{\dot{q}(t)\} \equiv \begin{Bmatrix} \dot{x}_1^{(1)}(t) \\ \dot{x}_3^{(1)}(t) \\ \dot{\theta}^{(1)}(t) \\ \dot{\varphi}^{(3/2)}(t) \end{Bmatrix} \tag{72}$$

The Cartesian velocities are linearly related to the generalised velocities using the B-matrix as follows:

$$\left\{\dot{X}(t)\right\} = \left[B(t)\right]\{\dot{q}(t)\} \tag{73}$$

The number of rows of the B-matrix is equal to the number of Cartesian velocities, while the number of columns is equal to the number of generalised velocities. In this case, the size of the B-matrix is 18×4:

$$[B(t)] = \begin{bmatrix} e_1 & e_3 & \underset{3x1}{0} & \underset{3x1}{0} \\ \underset{3x1}{0} & \underset{3x1}{0} & e_2 & \underset{3x1}{0} \\ e_1 & e_3 & R^{(1)}(t)\overleftrightarrow{s^{(2/1)}}^T e_2 & \underset{3x1}{0} \\ \underset{3x1}{0} & \underset{3x1}{0} & e_2 & \underset{3x1}{0} \\ e_1 & e_3 & B_{53} & B_{54} \\ \underset{3x1}{0} & \underset{3x1}{0} & \left(R^{(3/2)}(t)\right)^T e_2 & e_2 \end{bmatrix} \tag{74}$$

Where

$$B_{53} = R^{(1)}(t)\left\{\left(\overleftrightarrow{s^{(h/2)}}^T + \overleftrightarrow{s^{(2/1)}}^T\right) + R^{(3/2)}(t)\overleftrightarrow{s^{(3/h)}}^T\left(R^{(3/2)}(t)\right)^T\right\}e_2 \tag{75}$$

$$B_{54} = R^{(1)}(t)R^{(3/2)}(t)\overleftrightarrow{s^{(3/h)}}^T e_2 \tag{76}$$

and $\underset{3\times1}{0}$, e_1, e_2 and e_3 are defined as:

$$\underset{3\times1}{0} = \begin{pmatrix} 0 \\ 0 \\ 0 \end{pmatrix}, e_1 = \begin{pmatrix} 1 \\ 0 \\ 0 \end{pmatrix}, e_2 = \begin{pmatrix} 0 \\ 1 \\ 0 \end{pmatrix}, e_3 = \begin{pmatrix} 0 \\ 0 \\ 1 \end{pmatrix} \tag{77}$$

The derivation of the B-matrix concludes the kinematics of the system. A few points are made, in closure. A casual inspection of eqn. (74) reveals that the analysis can be greatly simplified by recognising the sparsity of this matrix. This could potentially reduce computational expenditure. However, the aim here is to solve this problem, while, at the same time, maintaining some form of generality to be used in future problems with more bodies and/or fewer restrictive assumptions on

the final motion (e.g. to account for yaw and roll). Thus, the form of the B matrix is maintained as is, without further simplifications. After the generalised coordinates are computed, the B matrix is used for computation of the Cartesian coordinates that enter into power and force calculations.

Note that the rotation matrix for the first float is not readily derivable (as is the case here with a simple pitch rotation about one axis). It would remain full as in eqn. (44) and would have to be solved for these terms at each time step. The procedure entails the use of the Cayley-Hamilton theorem to secure an implementation of the Rodriguez formula [1].

5 KINETICS OF THE M4 WAVE ENERGY CONVERTER

As this section addresses the kinetics it is reasonable to return to 3D generality for edification's sake.

5.1 Application of Analytical Mechanics

The Lagrangian, $Ł$, is a function that describes the state of a dynamic system in terms of generalised coordinates. A Lagrangian function is defined as the difference between the kinetic energy, *K*, and potential energy, *U*:

$$Ł^{(\alpha)}\left(q(t),\dot{q}(t),t\right)=K^{(\alpha)}\left(q(t),\dot{q}(t),t\right)-U^{(\alpha)}\left(q(t),t\right) \tag{78}$$

Next, the Action, *A*, is an integral of a function of time and space that outputs a scalar. Here, the Action is defined as the definite integral of the Lagrangian function over time:

$$A=\int_{t_0}^{t_1} Ł^{(\alpha)}\left(q(t),\dot{q}(t),t\right)dt \tag{79}$$

Hamilton's Principle states that "*the motion of a system occurs in such a way that the definite integral A becomes a minimum for arbitrary possible variations of the configuration of the system, provided the initial and final configurations of the system are prescribed"* [33].

Variation of The Action

To obtain the equations of motion, the variation of the Action is set equal to zero:

$$\delta\int_{t_0}^{t_1} Ł^{(\alpha)}\left(q(t),\dot{q}(t),t\right)dt=0 \tag{80}$$

Above, the variation symbol is considered as the derivative with respect to a variation parameter. This variation parameter commutes with the time derivative:

$$\frac{\partial q}{\partial t}=\dot{q}\Leftrightarrow\frac{\partial q}{\partial \delta}=\delta q \tag{81}$$

The variation parameter is a crucial part of being able to derive the equations of motion. The Gateaux derivative in functional space theory enables this variation.

It is necessary to first deal with the non-conservative forces. To include the non-conservative forces, the extension of Hamilton's Principle, known as the Principle of Virtual Work is exploited to accommodate non-conservative forces. Here, the Lagrangian is formulated as dependent only on the kinetic energy. All other forces (conservative or non-conservative) are accounted for as work, on the right side. The variation of The Action is rewritten as:

$$\int_{t_0}^{t_1} \delta K^{(\alpha)}\left(q(t),\dot{q}(t),t\right)dt = -\int_{t_0}^{t_1} \delta W^{(\alpha)}\left(q(t),\dot{q}(t),t\right)dt \tag{82}$$

This is a crucial relationship and is the basis for the equations of motion. From this point onwards, the dependencies of position and velocity are omitted for ease of notation. In order to derive the equations of motion the variation of the kinetic energy, $\delta K^{(\alpha)}(t)$, and the variation of the work, $\delta W^{(\alpha)}(t)$, must be found for insertion into eqn. (82). To find $\delta K^{(\alpha)}(t)$ and $\delta W^{(\alpha)}(t)$ in terms of generalised coordinates, another relationship for the B-matrix is revealed: The B-matrix that relates the Cartesian velocities $\{\dot{X}(t)\}$ to the generalised velocities $\{\dot{q}(t)\}$, also relates the variation of the Cartesian displacements $\{\delta\tilde{X}(t)\}$ to the variation of the generalised displacements $\{\delta q(t)\}$:

$$\left\{\delta\tilde{X}(t)\right\} = \left[B(t)\right]\left\{\delta q(t)\right\} \tag{83}$$

where the variation of the Cartesian displacements $\{\delta\tilde{X}(t)\}$ is defined as:

$$\left\{\delta\tilde{X}(t)\right\} \equiv \begin{Bmatrix} \delta x^{(1)}(t) \\ \left(\left(R^{(1)}(t)\right)^{T} \delta R^{(1)}(t)\right)_{\text{un}} \\ \delta x^{(2)}(t) \\ \left(\left(R^{(2)}(t)\right)^{T} \delta R^{(2)}(t)\right)_{\text{un}} \\ \delta x^{(3)}(t) \\ \left(\left(R^{(3)}(t)\right)^{T} \delta R^{(3)}(t)\right)_{\text{un}} \end{Bmatrix} \tag{84}$$

and the subscript "un" means that the matrix is un-skewed into a column vector. Therefore, the generality of the form of the B-matrix is retained. The general form leads to a general differential equation for all cases, distinguished only by the B-matrix.

Variation of Kinetic Energy

To find the variation of the kinetic energy in terms of generalised coordinates, the variation of the kinetic energy in cartesian coordinates is first found, before it is converted to generalised coordinates by applying eqn. (83).

The kinetic energy of each body in the system in cartesian coordinates is expressed by the angular momentum $\mathbf{H}^{(\alpha)}(t)$, and linear momentum $\mathbf{L}^{(\alpha)}(t)$:

$$\mathbf{H}^{(\alpha)}(t) = \boldsymbol{e}^{(\alpha)}(t)\, H^{(\alpha)}(t) = \boldsymbol{e}^{(\alpha)}(t)\, J^{(\alpha)}\omega^{(\alpha)}(t) \tag{85}$$

$$\mathbf{L}^{(\alpha)}(t) = \boldsymbol{e}^{I}\, L^{(\alpha)}(t) = \boldsymbol{e}^{I}\, m^{(\alpha)}\dot{x}^{(\alpha)}(t) \tag{86}$$

Here, $J^{(\alpha)}$ represents the moment of inertia matrix for body α. The total kinetic energy of a body α with the frame placed at the centre of mass is defined as:

$$K^{(\alpha)}(t) = \frac{1}{2}\left\{\dot{\mathbf{r}}^{(\alpha)}(t)\cdot\mathbf{L}^{(\alpha)}(t) + \boldsymbol{\omega}^{(\alpha)}(t)\cdot\mathbf{H}^{(\alpha)}(t)\right\} \tag{87}$$

For the whole system, the total kinetic energy in matrix form is expressed as:

$$K(t) = \frac{1}{2}\left\{\dot{X}(t)\right\}^T [M]\left\{\dot{X}(t)\right\}, \tag{88}$$

where the mass matrix [*M*] contains the masses and moments of inertia for each body in the system:

$$[M] \equiv \begin{bmatrix} m^{(1)}I_3 & \underset{3\times3}{0} & \underset{3\times3}{0} & \underset{3\times3}{0} & \underset{3\times3}{0} & \underset{3\times3}{0} \\ \underset{3\times3}{0} & J^{(1)} & \underset{3\times3}{0} & \underset{3\times3}{0} & \underset{3\times3}{0} & \underset{3\times3}{0} \\ \underset{3\times3}{0} & \underset{3\times3}{0} & m^{(2)}I_3 & \underset{3\times3}{0} & \underset{3\times3}{0} & \underset{3\times3}{0} \\ \underset{3\times3}{0} & \underset{3\times3}{0} & \underset{3\times3}{0} & J^{(2)} & \underset{3\times3}{0} & \underset{3\times3}{0} \\ \underset{3\times3}{0} & \underset{3\times3}{0} & \underset{3\times3}{0} & \underset{3\times3}{0} & m^{(3)}I_3 & \underset{3\times3}{0} \\ \underset{3\times3}{0} & \underset{3\times3}{0} & \underset{3\times3}{0} & \underset{3\times3}{0} & \underset{3\times3}{0} & J^{(3)} \end{bmatrix} \tag{89}$$

The variation of the kinetic energy in cartesian coordinates is expressed as:

$$\delta K(t) = \left\{\delta\dot{X}(t)\right\}^T [M]\left\{\dot{X}(t)\right\} \tag{90}$$

The components of the variation of the kinetic energy are still not defined. An appropriate expression for the variation of the Cartesian velocities $\{\delta\dot{X}(t)\}$ is:

$$\left\{\delta\dot{X}(t)\right\} \equiv \begin{Bmatrix} \delta\dot{x}^{(1)}(t) \\ \delta\omega^{(1)}(t) \\ \delta\dot{x}^{(2)}(t) \\ \delta\omega^{(2)}(t) \\ \delta\dot{x}^{(3)}(t) \\ \delta\omega^{(3)}(t) \end{Bmatrix} \tag{91}$$

For linear velocities, the variation of the time derivative is equal to the time derivative of the variation:

$$\delta\dot{x}^{(\alpha)}(t) = \frac{d}{dt}\delta x^{(\alpha)}(t) \tag{92}$$

For angular velocities, however, there is a restriction first proven by Holms [34] but reproduced using moving frames by Murakami [35].

$$\delta\omega^{(\alpha)}(t)=\frac{d}{dt}\left(\left(R^{(\alpha)}(t)\right)^{T}\delta R^{(\alpha)}(t)\right)_{\text{un}}+\overleftrightarrow{\omega^{(\alpha)}(t)}\left(\left(R^{(\alpha)}(t)\right)^{T}\delta R^{(\alpha)}(t)\right)_{\text{un}} \tag{93}$$

Making use of the previous two equations, eqn. (91) is written in compact form as:

$$\left\{\delta\dot{X}(t)\right\}=\frac{d}{dt}\left\{\delta\tilde{X}(t)\right\}+[D(t)]\left\{\delta\tilde{X}(t)\right\}, \tag{94}$$

where [*D(t)*] is a skew symmetric matrix that contains the angular velocity matrices for each frame:

$$[D(t)]\equiv\begin{bmatrix} \underset{3\times3}{0} & \underset{3\times3}{0} & \underset{3\times3}{0} & \underset{3\times3}{0} & \underset{3\times3}{0} & \underset{3\times3}{0} \\ \underset{3\times3}{0} & \overleftrightarrow{\omega^{(1)}}(t) & \underset{3\times3}{0} & \underset{3\times3}{0} & \underset{3\times3}{0} & \underset{3\times3}{0} \\ \underset{3\times3}{0} & \underset{3\times3}{0} & \underset{3\times3}{0} & \underset{3\times3}{0} & \underset{3\times3}{0} & \underset{3\times3}{0} \\ \underset{3\times3}{0} & \underset{3\times3}{0} & \underset{3\times3}{0} & \overleftrightarrow{\omega^{(2)}}(t) & \underset{3\times3}{0} & \underset{3\times3}{0} \\ \underset{3\times3}{0} & \underset{3\times3}{0} & \underset{3\times3}{0} & \underset{3\times3}{0} & \underset{3\times3}{0} & \underset{3\times3}{0} \\ \underset{3\times3}{0} & \underset{3\times3}{0} & \underset{3\times3}{0} & \underset{3\times3}{0} & \underset{3\times3}{0} & \overleftrightarrow{\omega^{(3)}}(t) \end{bmatrix} \tag{95}$$

By applying the B-matrix relationships (eqns. (73) and (83)) the variation of the kinetic energy in terms of generalised coordinates becomes:

$$\delta K(t)=\left\{\frac{d}{dt}[B(t)]\{\delta q(t)\}+[D(t)][B(t)]\{\delta q(t)\}\right\}^{T}[M][B(t)]\{\dot{q}(t)\} \tag{96}$$

The variation of the kinetic energy is ready for insertion into eqn. (82).

Variation of Work

The focus is turned to the *variation* of the work, also known as Virtual Work. To find the Virtual Work in terms of generalised coordinates, it is first defined in cartesian coordinates before it is converted to generalised coordinates by applying eqn. (83).

The Virtual Work done by the forces and moments in cartesian coordinates is expressed as:

$$\delta W = \left\{\delta \tilde{X}(t)\right\}^T \left\{F(t)\right\} \tag{97}$$

where the forces and moments acting on the three bodies of the M4 wave energy converter are defined as:

$$\left\{F(t)\right\} \equiv \begin{Bmatrix} F^{(1)}(t) \\ M^{(1)}(t) \\ F^{(2)}(t) \\ M^{(2)}(t) \\ F^{(3)}(t) \\ M^{(3)}(t) \end{Bmatrix} = \begin{Bmatrix} F_{hydro}{}^{(1)}(t) + F_{external}{}^{(1)}(t) \\ M_{hydro}{}^{(1)}(t) + M_{external}{}^{(1)}(t) \\ F_{hydro}{}^{(2)}(t) + F_{external}{}^{(2)}(t) \\ M_{hydro}{}^{(2)}(t) + M_{external}{}^{(2)}(t) \\ F_{hydro}{}^{(3)}(t) + F_{external}{}^{(3)}(t) \\ M_{hydro}{}^{(3)}(t) + M_{external}{}^{(3)}(t) \end{Bmatrix} \tag{98}$$

F_{hydro}(t) and M_{hydro}(t) are the total hydrodynamic forces and moments induced by waves (due to excitation, added mass and radiation damping), respectively. The external forces and moments, $F_{external}$(t) and $M_{external}$(t), come from hydrostatic stiffness, mechanical force from the PTO and gravitational forces. Forces are covered more in depth in section *6 - Hydrodynamics*.

Eqn. (83) is applied to rewrite eqn. (97) in terms of generalised coordinates:

$$\delta W = \left\{\delta q(t)\right\}^T \left\{F^*(t)\right\} \tag{99}$$

where the generalised force $\left\{F^*(t)\right\}$ is defined as:

$$\left\{F^*(t)\right\} = \left[B(t)\right]^T \left\{F(t)\right\} \tag{100}$$

5.2 Equations of Motion

The expressions obtained for the variation of the kinetic energy and the variation of the work are inserted into eqn. (82) to obtain the basis for the equations of motion in terms of generalised coordinates:

$$\int_{t_0}^{t_1}\left(\begin{array}{l}\left(\frac{d}{dt}\left\{\delta q(t)\right\}^T\left[B(t)\right]^T-\left\{\delta q(t)\right\}^T\left[B(t)\right]^T\left[D\right]\right)\left[M\right]\left[B(t)\right]\left\{\dot{q}(t)\right\}- \\ \left\{\delta q(t)\right\}^T\left\{F^*(t)\right\}\end{array}\right)dt=0 \tag{101}$$

After performing integration by parts on eqn. (101), and accounting for zero virtual displacement at the endpoints, second order coupled differential equations are obtained:

$$\left[M^*(t)\right]\left\{\ddot{q}(t)\right\}+\left[N^*(t)\right]\left\{\dot{q}(t)\right\}=\left\{F^*(t)\right\} \tag{102}$$

where the following terms are defined:

$$\left[M^*(t)\right]\equiv\left[B(t)\right]^T\left[M\right]\left[B(t)\right] \tag{103}$$

$$\left[N^*(t)\right]\equiv\left[B(t)\right]^T\left(\left[M\right]\left[\dot{B}(t)\right]+\left[D(t)\right]\left[M\right]\left[B(t)\right]\right) \tag{104}$$

Eqn. (102) is solved with respect to the list of generalised accelerations $\{\ddot{q}(t)\}$, to yield the following:

$$\left\{\ddot{q}(t)\right\}=\left[M^*(t)\right]^{-1}\left(\left\{F^*(t)\right\}-\left[N^*(t)\right]\left\{\dot{q}(t)\right\}\right) \tag{105}$$

This results in four coupled second order ordinary differential equations (ODEs), i.e. one for each generalised coordinate.

The F^*-term in eqn. (105) is the expression of the generalised forces; a similar statement can be made about the M^*-expression. Compared to traditional mechanics models, the extra term, $[N^*(t)]\{\dot{q}(t)\}$ in eqn. (105) occurs due to differences in *vectorial* mechanics and *analytical* mechanics. As described in eqn. (78) analytical dynamics requires one to formulate the kinetic and

potential energies of a system. As a result, there is no need for free-body diagrams. The N^*-term derives from the intersection of variational methods with the MFM and the variation of the angular velocities. This N^*-term is a statement that moment and virtual rotation are a natural pair to use in the Principle of Virtual work. Table 3 below distinguishes the vectorial and analytical approaches:

Table 3. Vectorial- versus analytical approaches

	***Vectorial* mechanics**	***Analytical* mechanics**
Applications	Simple applications	Complex applications
Founders	Newton	Lagrange and Hamilton
Structure	Vectors: momentum, force	Scalars: kinetic energy, potential energy, work
Basis	Laws	Principles

In order to solve the second order ODEs using numerical integration methods, the equations of motion are expressed as sets of coupled first order ODEs. This is done by first defining two new variables:

$$z_1 = q(t) \tag{106}$$

$$z_2 = \dot{q}(t) \tag{107}$$

Next step is to differentiate z_1 and z_2:

$$\dot{z}_1 = \dot{q}(t) = z_2 \tag{108}$$

$$\dot{z}_2 = \ddot{q}(t) = \left[M^*(t)\right]^{-1}\left\{F^*(t)\right\} - \left[M^*(t)\right]^{-1}\left[N^*(t)\right]\left\{z_2\right\} \tag{109}$$

This is simplified further by rewriting it as a single first order matrix differential equation:

$$\begin{bmatrix}\dot{z}_1\\ \dot{z}_2\end{bmatrix} = \begin{bmatrix}0 & 1\\ 0 & -\left[M^*(t)\right]^{-1}\left[N^*(t)\right]\end{bmatrix}\begin{bmatrix}z_1\\ z_2\end{bmatrix} + \begin{bmatrix}0\\ \left[M^*(t)\right]^{-1}\left\{F^*(t)\right\}\end{bmatrix} \tag{110}$$

This set of coupled first order ODEs is solved using a fourth order Runge-Kutta method. Lower order methods for solving the ODEs could also be applied since the equations are only of second order. Using lower order integration methods may allow for small improvements in computational efficiency whilst giving similarly accurate results. Examples of lower order numerical integration schemes that can be used are Beeman's algorithm, Verlet integration, Midpoint method, Newmark-beta method and others. Nevertheless, the Runge-Kutta numerical method is used because it is straight forward to implement and it has previously been used together with the MFM [2].

5.3 The Runge-Kutta numerical method

For a first order differential equation, $\dot{y} = f(t, y)$, the fourth order Runge-Kutta numerical method (RK4) estimates the next value y_{n+1} by using the previous value y_n plus the weighted average of four increments, where h is the step size [36]. This integration scheme is implemented using MATLAB.

$$k_1 = f\left(t_n, y_n\right) \tag{111}$$

$$k_2 = f\left(t_n + \frac{h}{2}, y_n + \frac{h}{2}k_1\right) \tag{112}$$

$$k_3 = f\left(t_n + \frac{h}{2}, y_n + \frac{h}{2}k_2\right) \tag{113}$$

$$k_4 = f\left(t_n + h, y_n + hk_3\right) \tag{114}$$

$$y_{n+1} = y_n + \frac{h}{6}\left(k_1 + 2k_2 + 2k_3 + k_4\right) \tag{115}$$

6 HYDRODYNAMICS

Analysing the hydrodynamics of WECs is a non-trivial task due to the complexity of the interacting forces that take place. The first theoretical developments performed such analyses in the frequency-domain. Accordingly, frequency dependent hydrodynamic coefficients to describe the excitation, radiation and hydrostatic forces were defined, found with the aid of computer codes based on the boundary element method [7].

It is of interest to study devices in the time-domain due to phase-dependent effects – such as non-linear hydrodynamic interactions in addition to evaluating non-linear control strategies of the power-take-off for smoothing power output [37]. These phase dependencies are also important for the proper assessment of device loads, such as for fatigue limit state design and for preliminary dimensioning of structures [38].

W. E. Cummins established a time-domain model that represents motion response of a marine structure subject to a linearly superposed sea-state of regular waves and separates the variables into individual units, such as by removing dependency of added mass on frequency [39]. The only assumption required (aside from convergence) is linearity, and experimental data indicate that the assumption is a good working approximation for small to moderate oscillations [39]. Furthermore, this assumption means that any excitation, periodic or non-periodic, continuous or discontinuous, is permissible, so long as it results in small displacements [39]. Following Cummins' linearization, the equations of motion for a floating body with zero forward speed in the time-domain are [39]:

$$\left(m_{ij} + A_{ij}^{\infty}\right)\ddot{x}_i(t) + \int_{-\infty}^{t} L_{ij}(t-\tau)\dot{x}_i(\tau)d\tau + c_{ij}x_i(t) = f_d(t) + f_{ext} \tag{116}$$

where

- i and j denote mode with all combinations for surge, heave and pitch for the floats
- $x_i(t)$, $\dot{x}_i(t)$, $\ddot{x}_i(t)$ = position, velocity and acceleration of the floats
- m_{ij} = mass and inertia of the floats
- $f_d(t)$ = excitation force (*section 6.1*)

- $\int_{-\infty}^{t} L_{ij}(t-\tau)\dot{x}_i(\tau)d\tau$ = radiation force (*section 6.2*)
- A_{ij}^{∞} = added mass at infinite frequency (*section 6.3*)
- c_{ij} = hydrostatic stiffness matrix (*section 6.4*)
- f_{ext} = external forces (e.g. viscous drag, mechanical force from the PTO system and gravitational force) (*section 6.4*)

This time-domain model produces time-series results and is an appropriate tool for studies of converters in irregular waves [7].

6.1 Excitation Forces

$$\left(m_{ij} + A_{ij}^{\infty}\right)\ddot{x}_i(t) + \int_{-\infty}^{t} L_{ij}(t-\tau)\dot{x}_i(\tau)d\tau + c_{ij}x_i(t) = \boxed{f_d(t)} + f_{ext} \quad (117)$$

The wave excitation force (red box in eqn. (117)) occurs due to incident waves, visualised in Figure 19:

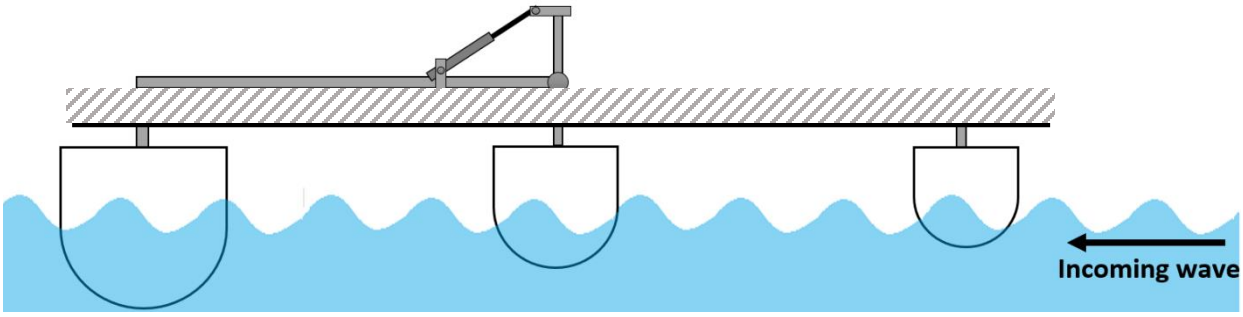

Figure 19. Hydrodynamic forces acting on the fixed body, when the device is unable to move, while waves travel towards the body. These forces are referred to as wave excitation forces.

The wave excitation force is formed by the Froude-Krylov force, obtained by integration of the pressure field from undisturbed waves, and diffraction force from wave scattering due to the presence of the body. By assuming that the excitation force generated by an incident wave is a harmonic function that is directly proportional to the wave amplitude, the most straightforward procedure to model first-order wave forces in irregular waves is the simple linear superposition of *N* independent sinusoidal components [37]. Figure 20 visualises the principle of superposition

where independent sinusoidal components (dotted lines) are simply added together to achieve the combined wave (solid line).

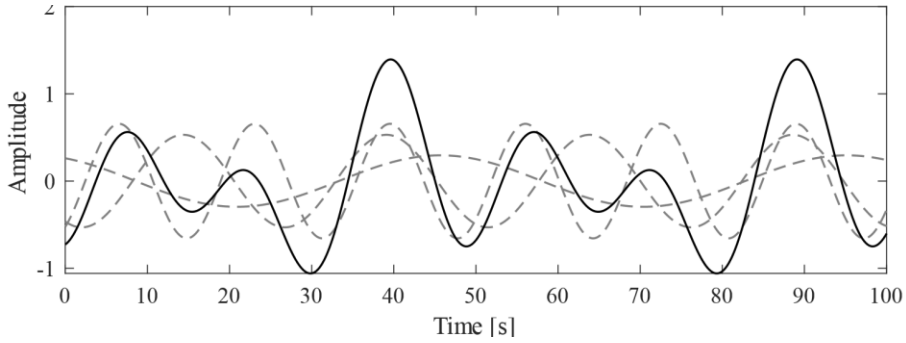

Figure 20. Wave superposition with sinusoidal components (dotted lines) and combined wave (solid line).

The first order excitation force is given as:

$$f_d(t) = \sum_{i=1}^{N} f_e\,(\omega_i) A_i \cos(\omega_i t + \phi(\omega_i) + \varphi_i) \tag{118}$$

where the frequency dependent $f_e(\omega)$, which is an excitation force coefficient, and $\phi(\omega)$, which is a phase angle, are extracted directly from a diffraction model. The excitation force is directly proportional to the wave amplitude, A_i. The phase angle represents the difference in time between a peak in the incident wave profile at the centre of the device and a peak of the excitation force. The information on the phase angle is very important in systems with multiple degrees of freedom because of the difference in phases between the excitation forces acting on each degree of freedom. Assuming that individual wave components are statistically independent [40], the wave surface elevation phases, φ_i, are randomly selected within [0;2π]. With this assumption, the randomness of the elevation process is properly reproduced and its statistical properties are correctly modelled [37].

6.2 Radiation Forces

$$\left(m_{ij} + A_{ij}^{\infty}\right)\ddot{x}_i(t) + \boxed{\int_{-\infty}^{t} L_{ij}(t-\tau)\dot{x}_i(\tau)d\tau} + c_{ij}x_i(t) = f_d(t) + f_{ext} \tag{119}$$

The radiation force (red box in eqn. (119)) occurs due to body motion radiating waves away, visualised on still water (no incident waves) in Figure 21:

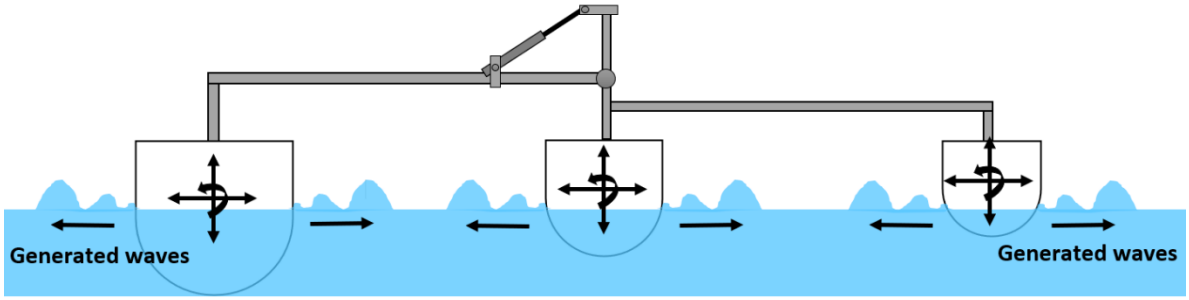

Figure 21. Radiation forces acting on the body when it is forced to oscillate on otherwise still water.

The radiation force consists of a convolution integral that is associated with fluid memory effects and is depend on past time, τ [39]. $B_{ij}(\omega)$ is the amplitude of the in-phase and out-of-phase components of the response to a unit amplitude forcing function of frequency, ω [39]. This is pre-computed in a panel code (WAMIT – [3]). The radiation impulse response function, $L_{ij}(t)$, is related to $B_{ij}(\omega)$ by

$$L_{ij}(t) = \frac{2}{\pi}\int_0^\infty B_{ij}(\omega)\cos(\omega t)\,d\omega \tag{120}$$

using Fourier inversion formulas [39]. The radiation forces are radiated away from the floats and are consequently opposite in sign compared to the excitation forces.

6.3 Added Mass Forces

$$\left(m_{ij} + A_{ij}^{\infty}\right)\ddot{x}_i(t) + \int_{-\infty}^{t} L_{ij}(t-\tau)\dot{x}_i(\tau)d\tau + c_{ij}x_i(t) = f_d(t) + f_{ext} \tag{121}$$

The forces from added mass (red box in eqn. (121)) occur because of the inertia of the water surrounding the body [7]. In order to simulate time-dependent motion of an irregular sea-state, the added mass at infinite frequency is used following Cummins [39] in order to decouple the dependency of added mass on frequency. This value is pre-computed in a panel code, WAMIT [37], as:

$$A_{ij}^{\infty} = \lim_{\omega\to\infty} A_{ij}(\omega) \tag{122}$$

6.4 Hydrostatic Restoring Forces and External Forces

$$\left(m_{ij} + A_{ij}^{\infty}\right)\ddot{x}_i(t) + \int_{-\infty}^{t} L_{ij}(t-\tau)\dot{x}_i(\tau)d\tau + \boxed{c_{ij}x_i(t)} = f_d(t) + \boxed{f_{ext}} \tag{123}$$

The term in the left-most red box in eqn. (123) is the hydrostatic restoring force. This is the force on a body due to the change in hydrostatic pressure on the wetted surface of the body as it moves from its equilibrium position [39]. Surge displacement provides no restoring forces; the restoring forces are only computed for heave and pitch displacements:

$$V_{rest} = -\rho g \pi r^2 z \tag{124}$$

$$M_{rest} = -\rho g \pi \frac{r^4}{4}\theta \tag{125}$$

where *r* is float radius and *z* is defined zero at the still water level and positive upwards.

The external forces (right-most red box in eqn. (123)) occur due to viscous drag, mechanical force from the PTO system and gravitational forces.

The viscous drag force acts in the opposite direction to the relative motion of an object with respect to the fluid. This force is computed by integration over the wetted surface area, *S*:

$$f_{drag}(t) = \int SdF = \frac{1}{2}\rho A_{wet} C_D \dot{x}|\dot{x}| \tag{126}$$

Where A_{wet} is the projected area, C_D is the drag coefficient and $\dot{x}$ is the relative fluid velocity. However, prior research shows that rounded float bases give minimal drag losses and drag coefficients in heave are less than 0.3 ([3], [41]). The drag force is therefore neglected in this study.

Mechanical force in the actuator is converted to a moment about the hinge by multiplying the lever arm and is modelled as a linear damper [3]. The moment from the actuator is computed by multiplying a damping coefficient, B_{PTO}, with the relative angular velocity of the floats:

$$M_{PTO}(t) = -B_{PTO}\left(\omega^{(1)}(t) - \omega^{(3)}(t)\right) \tag{127}$$

From the actuator moment, $M_{PTO}(t)$, the power output is computed by multiplying the relative angular velocity of the floats:

$$P_{tot} = M_{PTO}\left(\omega^{(1)}(t) - \omega^{(3)}(t)\right) \tag{128}$$

6.5 Total Force

As visualised in Figure 22, eqn. (116) is directly inserted into F^* of the equations of motion found using the MFM, eqn. (105), where M^* and its corresponding rotation matrices move the forces to the mass centres of each float.

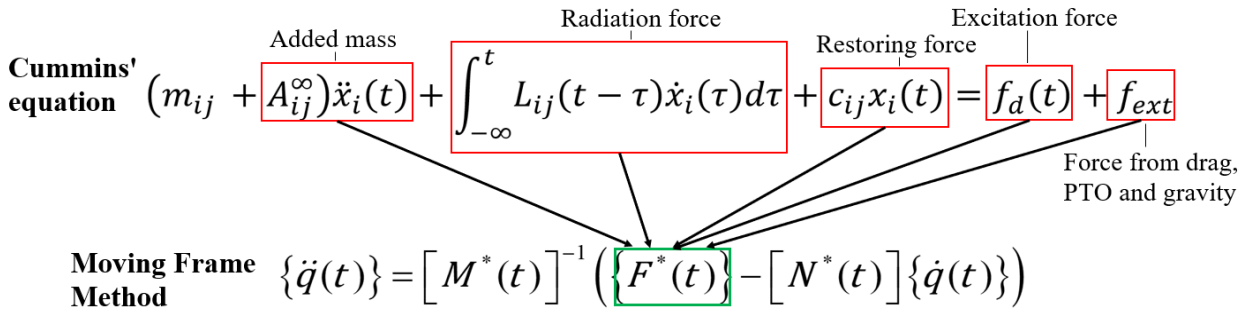

Figure 22. Cummins' equation and the MFM

What remains before being able to solve the equations of motion, is the required hydrodynamic coefficients.

6.6 Hydrodynamic Coefficients

In order to eliminate a possible source of error, added mass, diffraction and radiation coefficients are taken from the same WAMIT diffraction model from [3]. The moments from WAMIT are generated about the centre of flotation ([42]), whereas the MFM requires all forces and moments about the centre of mass. This small translation is neglected in this work; however, it is noted that this could cause some small discrepancies between the MFM and the earlier results of [3]. Figure 23 illustrates how the coefficients are incorporated for computation of the forces – with the forces inserted into the right-hand side of the equation found with the MFM.

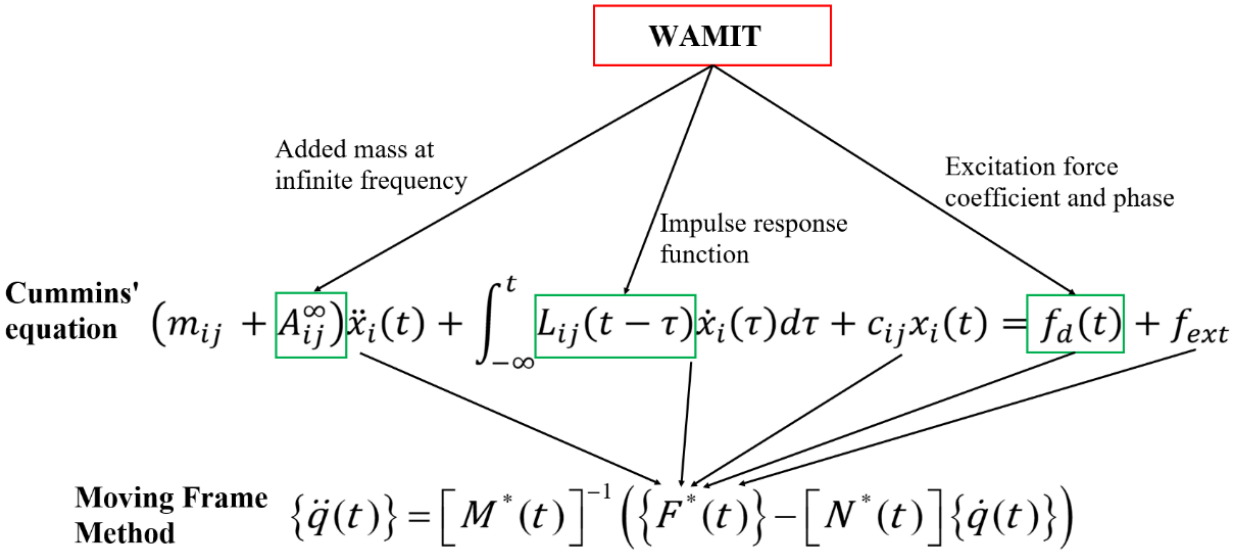

Figure 23. Implementation of hydrodynamic coefficients into the Moving frame method.

6.7 Code Structure

The MFM model is created in MATLAB due to its simplicity in matrix manipulation. First the equations of motion are found using the MFM, followed by preparing the input wave spectrum and importing all hydrodynamic coefficients from the WAMIT diffraction model from [3]. The coupled differential equations are solved by applying a fourth order Runge-Kutta numerical method. All forces are computed at every iteration in the Runge-Kutta loop. Figure 24 visualises the code structure:

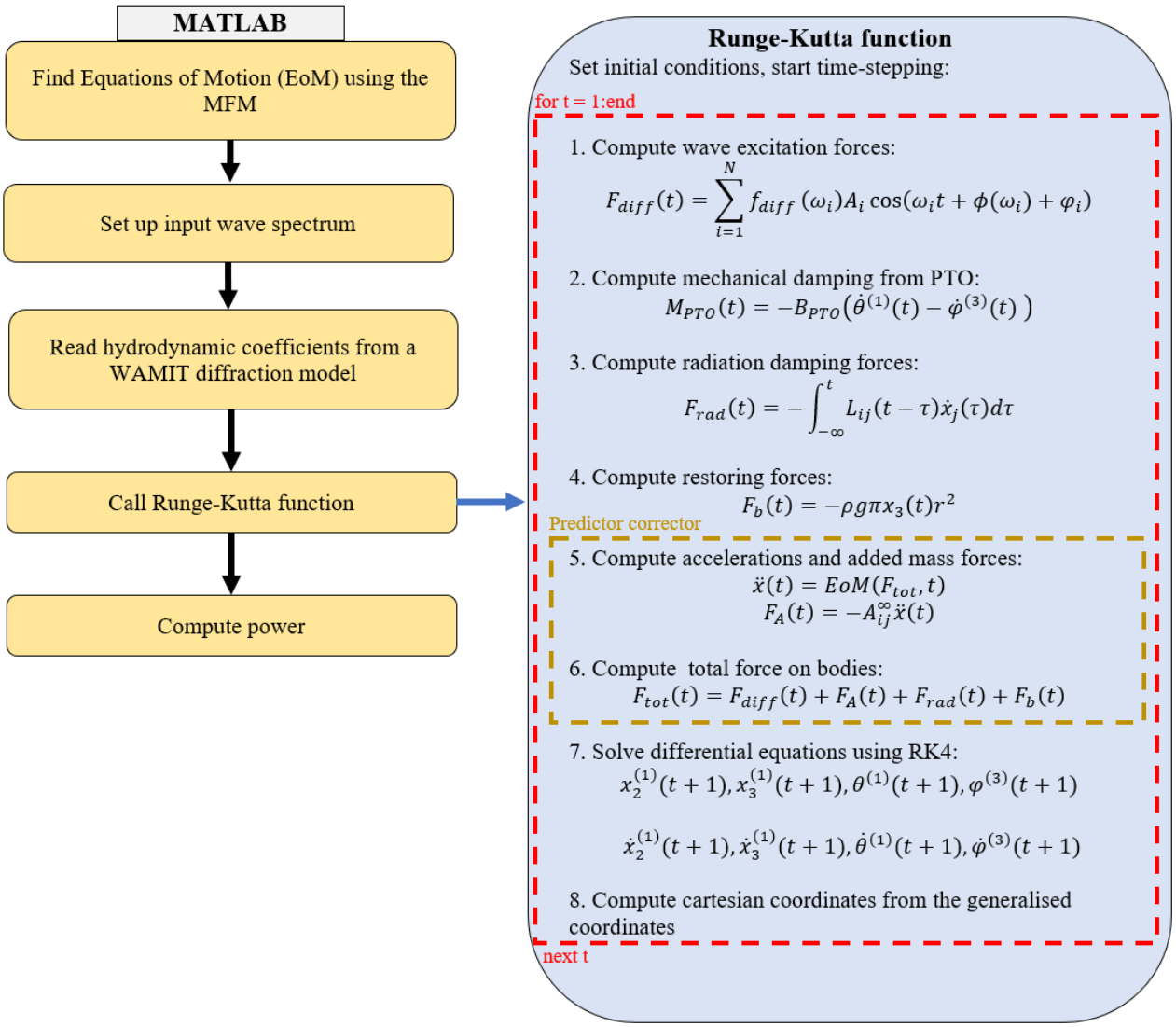

Figure 24. Code flowchart

The predictor corrector loop (yellow dotted box inside the Runge-Kutta function in Figure 24) is required because accelerations are dependent on forces and added mass forces are dependent on accelerations, therefore using values directly leads to instabilities in the code. A sensitivity analysis is conducted to determine the number of iterations required through the correct loop. Figure 25 shows for the vertical force calculated on float 3 at time, t=100 s, that approximately 10 iterations are required for convergence.

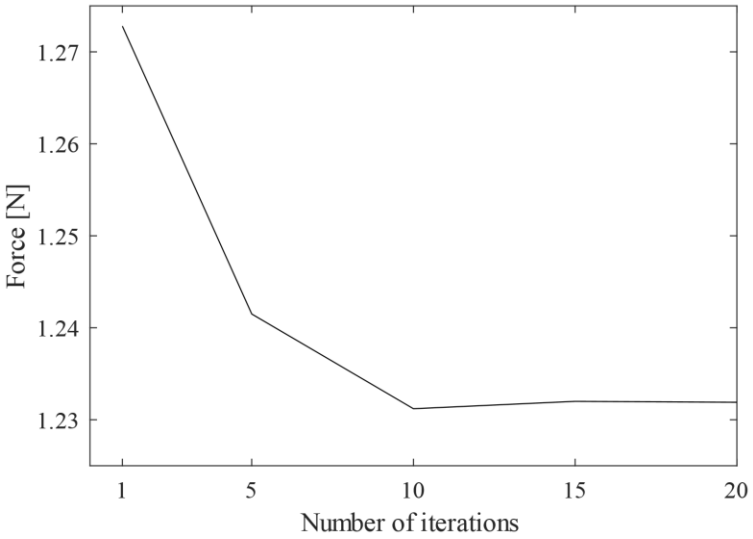

Figure 25. Sensitivity analysis of corrector loop

7 RESULTS & DISCUSSION

The results obtained from the analyses of a model-scale three-float M4 device are presented for irregular sea spectra, specified with significant wave height, $H_s = 0.04$ m, peak wave period, T_p, in the range 0.7-1.8 s and peakedness parameter $\gamma = 3.3$ (JONSWAP) and $\gamma = 1$ (Pierson-Moskowitz). The results are compared with an experimentally-validated vectorial mechanics model from [3]. From the excitation force in Figure 26, it is clear that the input wave trains are identical in both models; this is because the same random numbers are used for generating the wave elevation. In all the time-domain figures a 20 s sample of the full 120 s time-series is shown.

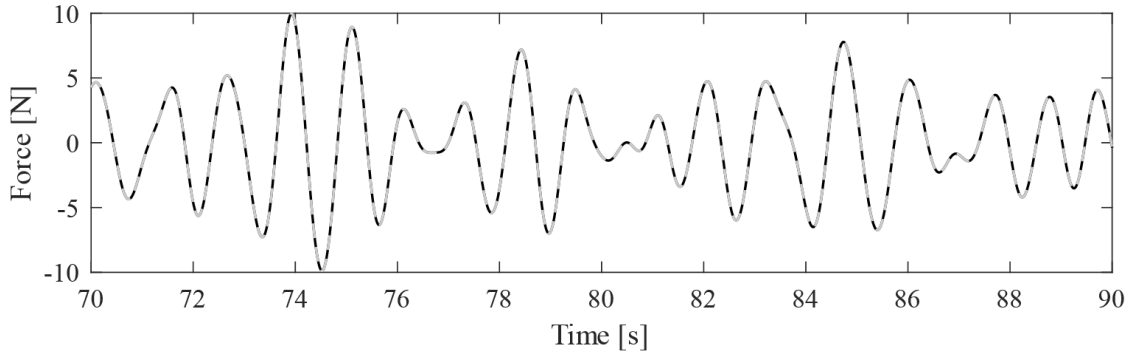

Figure 26. Vertical excitation force for $T_p = 1.2$ s, $\gamma = 1$ as calculated by the vectorial model (dashed) and MFM (solid)

The following analyses are conducted in order to compare the MFM model to the vectorial mechanics model:

Analysis 1 Compare time-domain results; added mass force, radiation force, heave and surge response on float 3 for one sea-state ($H_s = 0.04$ m, $T_p = 1.2$ s, $\gamma = 1$).

→ This indicates whether the hydrodynamic forces are successfully implemented into the MFM or not.

Analysis 2 Compare frequency-domain results; power capture and θ_{rms} for a range of sea-states ($H_s = 0.04$ m, $T_p = 0.7$-1.8 s, $\gamma = 3.3$).

→ This validates the MFM model for a range of sea states and enables analyses at various sites.

Analysis 3 Compute full-scale energy yield at a site using Froude scaling.

→ This demonstrates the full-scale potential of the M4 device of interest to the reader.

7.1 Analysis 1: Time-domain results

For comparison with results from [3], analysis 1 uses a Pierson-Moskowitz spectrum as the input wave spectrum. The time-series of vertical added mass and radiation forces acting on float 3 are first compared to ensure correct implementation of these forces into the MFM (Figure 27 and Figure 28). Note that the dominant diagonal added mass terms are not included in Figure 27 and that restoring forces are not shown due to lack of available data from [3] to compare this with.

For computation of the radiation force (Figure 28), the impulse response function is pre-computed with the convolution integral being directly integrated to four peak periods in advance of the current time-step [3]. The frequency-dependent radiation damping, $B(\omega)$, is pre-computed in WAMIT for a set of 200 frequency intervals evenly spaced between 0 and 4 Hz.

Finally, the resulting heave and surge response of float 3 is computed and compared with the vectorial mechanics model (Figure 29).

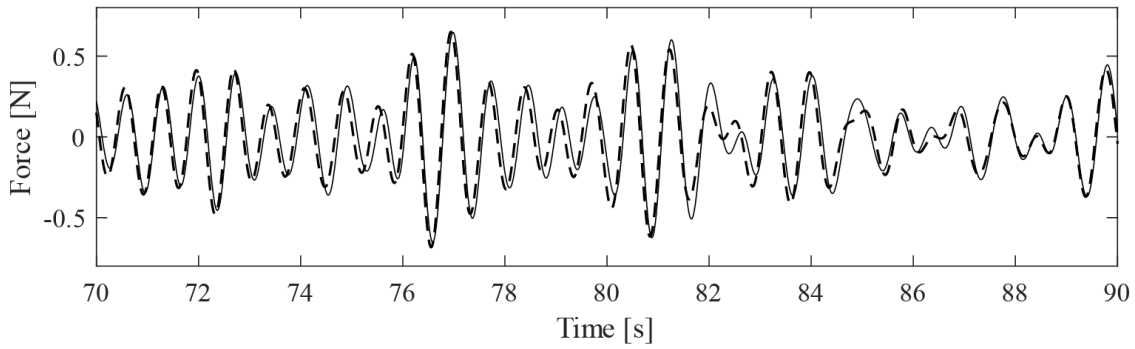

Figure 27. Vertical added mass force for $T_p = 1.2$ s as calculated by the vectorial model (dashed) and MFM (solid)

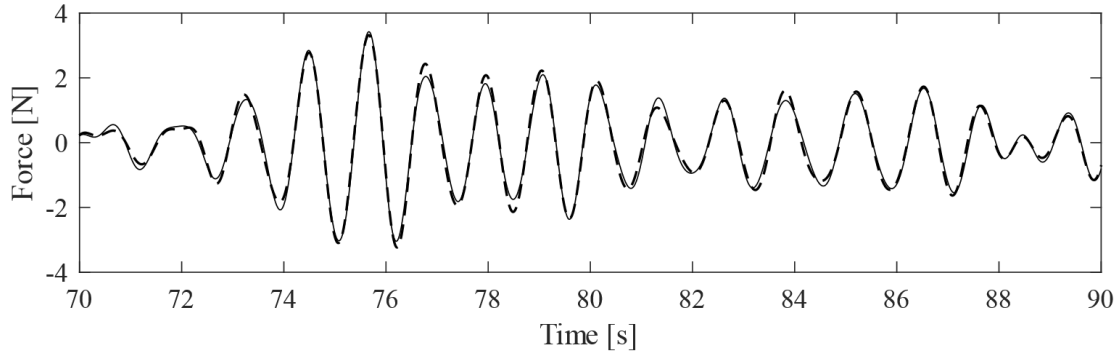

Figure 28. Vertical radiation force for $T_p = 1.2$ s as calculated by the vectorial model (dashed) and MFM (solid)

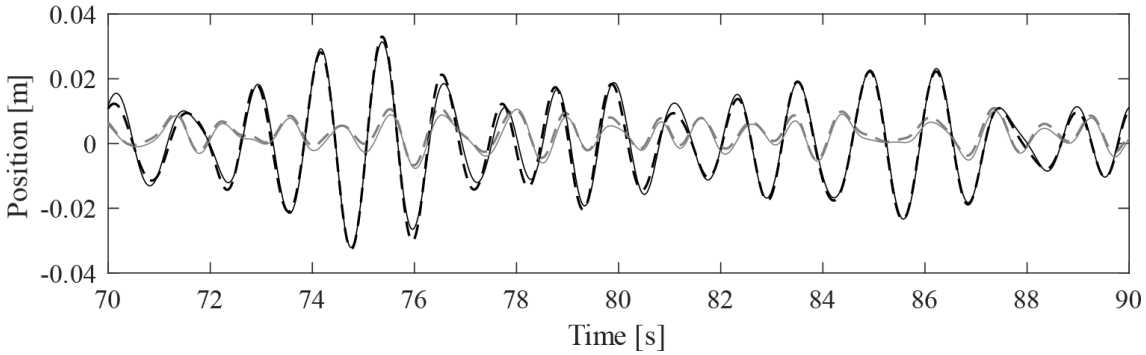

Figure 29. Heave (black) and surge (grey) position for $T_p = 1.2$ s as calculated by the vectorial model (dashed) and MFM (solid).

The added mass and radiation forces from the MFM model show near-identical agreement to the experimental-validated vectorial mechanics model from [3] (Figure 27 and Figure 28). The root-mean-square error, RMSE, is calculated as eqn. (11) to give a quantitative measure of the discrepancy. RMSE values between the two models are less than 8×10^{-2} N and 1.5×10^{-1} N for added mass and radiation, respectively. The resulting heave and surge response on float 3 also show close agreement (Figure 29) with RMSE values less than 3×10^{-3} m and 4×10^{-3} m, respectively.

The small discrepancies arise due to the following:

- This work uses a fourth order Runge-Kutta method for solving the differential equations, while the vectorial mechanics model from [3] uses Beeman's method.
- Hydrodynamic coefficients are defined about the centre of flotation and not centre of mass, which is required in the MFM model. Due to the small relative rotations of the floats at these periods, the model is likely to be more sensitive to translational errors.

These results indicate that the hydrodynamic forces in an example irregular sea-state are successfully implemented into the MFM.

7.2 Analysis 2: Frequency-domain results

It is of interest to validate the MFM model for a range of sea-states and enable analyses at various sites. For comparison with results from [3], analysis 2 uses a JONSWAP spectrum as the input wave spectrum. From eqns. (9), (10) and (128) the power capture, CWR and θ_{rms} for a range of sea-states are computed and compared to the vectorial mechanics model as seen in Figures 30-32.

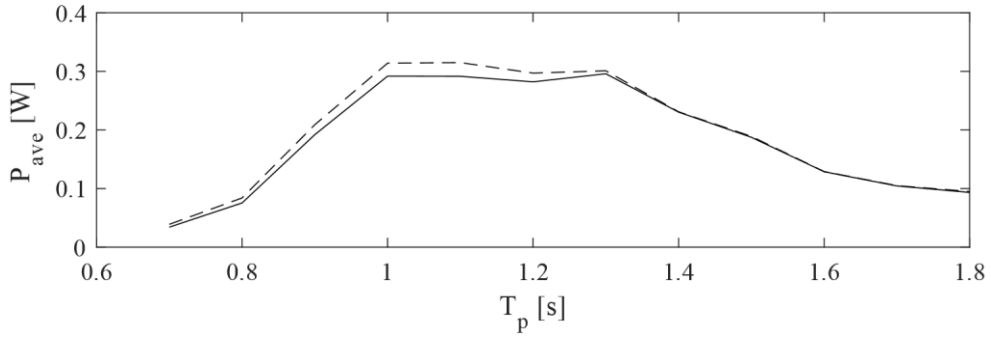

Figure 30. Average power generation for H_s=0.04 m as calculated by the vectorial model (dashed) and MFM (solid)

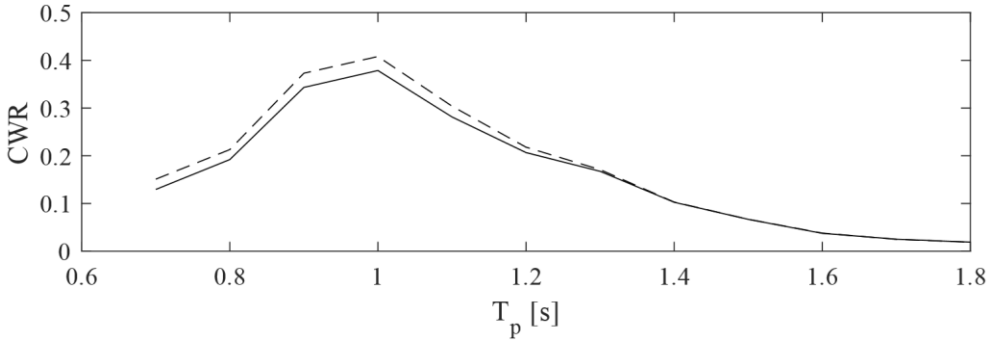

Figure 31. Capture-width ratio for H_s=0.04 m (black) as calculated by the vectorial model (dashed) and MFM (solid)

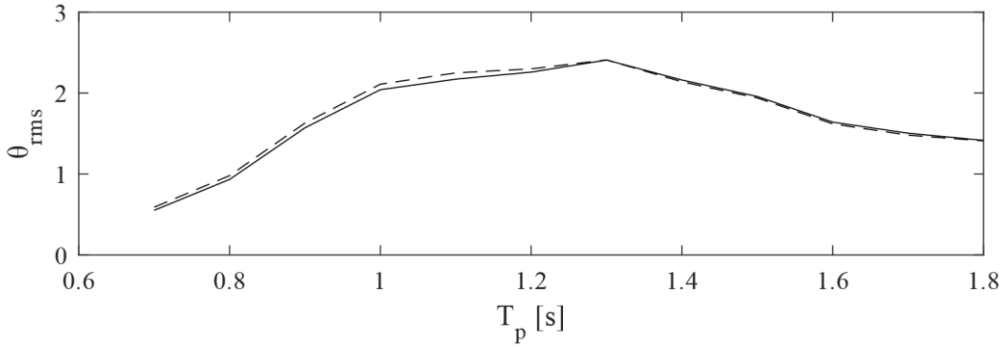

Figure 32. Variation of θ_{rms} (degrees) for H_s=0.04 m as calculated by the vectorial model (dashed) and MFM (solid)

Power capture and θ_{rms} from the MFM model show close agreement to the experimental-validated vectorial mechanics model from [3] across the full range of spectra with only a slight underprediction (<7%) of power at periods shorter than 1 s (Figure 30 and Figure 32) due to the reasons listed in analysis 1. Figure 31 shows a high capture-width ratio (>0.3) for several peak periods, suggesting good power capture and also in agreement with [3]. This validates the MFM model for a range of sea states and enables analyses at various sites.

7.3 Analysis 3: Full-scale results at a site in Ireland

For scaling results from model-scale to full-scale an optimum scaling factor of 70 is used for the site at Belmullet in Ireland [3]. Applying eqns. (3-4), all peak periods and wave heights in Table 1 are scaled from full-scale to model-scale in order to find average power capture for all sea-states. The full-scale average power is computed by applying eqn. (2). Next, the annual energy yield for each sea-state is found using eqn. (8) and the probability of occurrence from Table 1, presented in Figure 33. Finally, the total annual energy yield is computed.

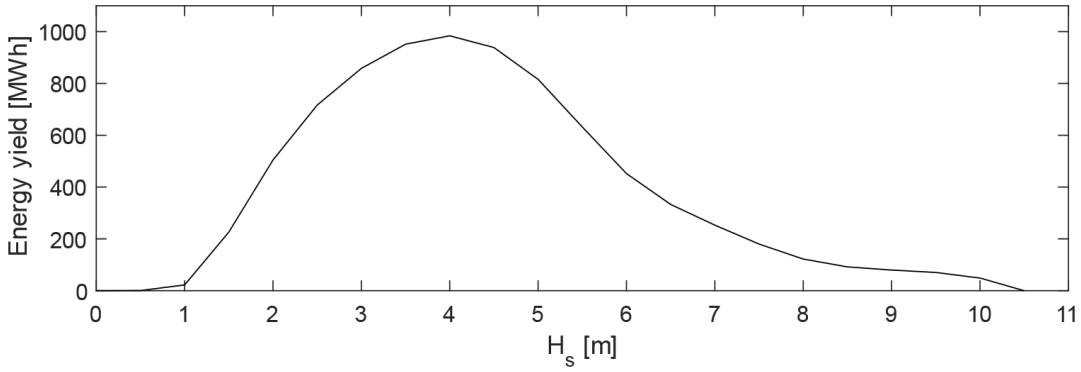

Figure 33. Energy yield at Belmullet [3] as a function of significant wave height

This gives a total annual energy yield of 8282 MWh which is within 3% of the value calculated using the vectorial mechanics model [3]. The average power and capacity are consequently 945 kW and 2.84 MW, respectively. The results are hence less sensitive than the underprediction of average power from analysis 1 because for this site there are several sea state occurrences at peak periods greater than $T_{Pm} = 1$ s. Other sites may have different sensitivity depending on the probability distribution of H_s and T_P.

The same procedure has been done earlier in [3] for various sites and device configurations and is presented in Table 4 for the site at Belmullet for the three-float and eight-float configurations.

Table 4. Power and energy estimate for the site in Ireland with scatter diagram from [27]

Configuration	Average power [kW]	Annual energy yield [MWh]	Rated power [MW]
3fl_111 (MFM)	945	8282	2.84
3fl_111 (from [3])	970	8505	2.91
8fl_134 (from [3])	2998	26264	8.99

The results show an increase in capacity by a factor of three for an increase from three to eight floats. The vectorial mechanics model from [3] has also found that optimum device capacities for the eight-float configuration range between 3.7 MW and 17.8 MW depending on the site resource. Compared to offshore wind turbines where currently capable capacities are of the order of 10 MW, this suggests the M4 has a competitively high-power capability. Levelized cost of energy is computed in [3] based on relative changes in capital cost for several sites and device configurations and is shown to be less than 10 pence/kWh. Due to other sensitivities, such as operations and maintenance, cost is not addressed further in this work.

Although several device configurations of the M4 have been analysed, it is probable that other configurations have better characteristics and that indeed the best configuration may be site dependent [3]. It is therefore useful to find optimal device arrangements and float sizes relative to the site-specific resource. However, cost benefits also exist for mass unit production of a standard solution that effectively extracts energy in all cases. Effective optimisation algorithms can accommodate a wide range of input parameters which would otherwise not be possible to evaluate effectively by intuition alone. Such optimisation nevertheless requires rapid calculation of many device layouts and parameters, which the extensibility of the MFM may enable.

The MFM has successfully modelled a multi-body WEC in irregular sea-states and can therefore be taken further in more detailed analysis with larger float configurations and more complex wave energy converters.

7.4 Approach

One way to model the 111-configuration of the M4 device using the MFM is to ‘merge’ the bow and mid float into one body because they move together in pitch – however, this research has shown the usefulness of an additional moving frame. Even though the moving frame at the mid float always has the same angular motion as the frame at the bow float, the analysis is greatly simplified because all the moment-arms from the hydrodynamic forces are mechanically accounted for through the rotation matrices in the equations of motion. The alternative, using two frames instead of three, gives the same result, but the moment-arms would in that case have to be computed manually. This is time consuming and, as was experienced through this work, allows for additional human- or coding errors.

It is possible to conduct this work without recourse to SE(3). The beauty of the MFM is the consistent notation from 2D and 3D single-bodies and multi-bodies. Thus, in this simple 3-body case, it is straightforward to conduct this work using three single bodies, with a vectorial mechanics model. However, using SE(3) enables analyses which can be readily scaled up to larger configurations in all six degrees of freedom, without increasing notational complexity. Note that modelling farms of devices requires the hydrodynamics of the whole farm to be modelled, such as to include shadowing effects.

8 CONCLUSION

In this project hydrodynamic forces have been, for the first time, implemented into the MFM and a multi-body WEC in irregular sea-states has been successfully modelled using this method.

The equations of motion have been derived by utilising the Special Euclidean Group SE(3). This maintains a notation that is consistent from 2D and 3D single bodies to multi-bodies allowing for an analysis which can be readily scaled up to include multiple links, bodies, and farms of devices, without increasing notational complexity and without loss of generality.

This work has modelled the three-float M4 WEC subject to irregular wave spectra using the MFM and linearization by Cummins' equation. Preliminary model-scale results were compared to an experimentally-validated vectorial mechanics model of [3] showing excellent agreement, with a root-mean square error of the time-series in heave and surge response of less than 4×10^{-3} m. Power capture and θ_{rms} for the model-scale device showed close agreement across all peak periods with only a slight underprediction (<7%) of power at peak periods shorter than 1 s. Some discrepancies between the model-scale results and earlier experimental work were found and this is attributed to moments from the WAMIT diffraction model generated about centre of flotation and not centre of mass, which is required in an MFM model. Nevertheless, results for full-scale annual energy yield for a demonstrative site in Ireland [27] were within 3% of that calculated using the vectorial mechanics model of [3], highlighting that sensitivity to the underprediction in power is small when considering the spread of availability of power with wave period. The results validate the MFM model and show that hydrodynamic forces in irregular sea-states have been successfully implemented.

Previous work from [3] has found that the M4 device capacity increases by a factor of three for an increase from three to eight floats and that the device can reach up to 17.8 MW for an eight-float configuration, which is indicative of the high performance of the M4 device.

The presented work indicates that the MFM can effectively be used for analysis of more complex wave energy converters in all six degrees of freedom while also enabling further optimisation studies of the M4 device.

9 FUTURE WORK

Future work will build upon this work and utilise the MFM for evaluating larger float configurations of M4. Hydrodynamic coefficients will be defined about the centre of mass in order to avoid discrepancies in power estimation. Furthermore, the method will be used within an optimisation strategy to optimise device arrangements and float sizes given a specific site resource. The MFM will also be applied to other complex wave energy converters in all six degrees of freedom.

The computational efficiency of the MFM compared to vectorial mechanics should also be assessed to evaluate the potential for more efficient computations and the possibility to incorporate more complex, non-linear wave theories. Furthermore, the method plans to be coupled with a finite element model for evaluating structural loads and mooring line loads.

10 REFERENCES

[1] J. Nyland, H. Teigland and T. Impelusso, “Use of the Moving Frame Method in Dynamics to Model Gyroscopic Control of Small Crafts at Sea: Theory - Part 1,” *ASME International Mechanical Engineering Congress and Exposition, paper ID IMECE2017-70108,* 2017.

[2] J. Nyland, H. Korsvik, E. Rognsvåg, T. Tomren and T. Impelusso, “Dual Gyroscope Wave Energy Converter,” *ASME International Mechanical Engineering Congress and Exposition, paper ID IMECE2019-10266,* 2019.

[3] P. Stansby, E. C. Moreno and T. Stallard, “Large capacity multi-float configurations for the wave energy converter M4 using a time-domain linear diffraction model,” *Applied Ocean Research Volume 68,* pp. 53-64, 2017.

[4] European Commission, “A Clean Planet for all - A European strategic long-term vision for a prosperous, modern, competitive and climate neutral economy,” Brussel, 2018.

[5] United Nations, “Transforming our world: The 2030 agenda for sustainable development A/RES/70/1,” 2015.

[6] J. Falnes, “A review of wave-energy extraction,” in *Marine Structures Volume 20(4)*, Elsevier Ltd., 2007, pp. 185-201.

[7] A. Falcao, “Wave energy utilization: A review of the technologies,” in *Renewable and Sustainable Energy Reviews Volume 14*, Elsevier Ltd., 2010, pp. 899-918.

[8] J. Falnes, “Research and development in ocean-wave energy in Norway,” *International symposium on ocean energy development,* 1993.

[9] Y. Washio, H. Osawa, Y. Nagata, F. Fujii, H. Furuyama and T. Fujita, “The Offshore Floating Type Wave Power Device "Mighty Whale": Open Sea Tests,” *Proceedings of tenth International Offshore and Polar Engineering Conference, Seattle; Volume 1,* 2000.

[10] P. J. Kofoed, P. Frigaard, E. Friis-Madsen and C. H. Sørensen, “Prototype testing of the wave energy converter Wave Dragon,” in *Renewable Energy Volume 31(2)*, Elsevier Ltd., 2006, pp. 181-189.

[11] L. C. Iversen and P. M. Lillebekken, “Model test of a scale 1:10 phase-controlled wave-power buoy of type N2 in the sea,” Norges teknisk-naturvitenskapelige universitet, Fakultet for naturvitenskap og teknologi, Institutt for fysikk, 1983.

[12] R. Yemm, D. Pizer, C. Retzler and R. Henderson, “Pelamis: experience from concept to connection.,” *The peaks and troughs of wave energy, the dreams and the reality Volume 370(1959),* pp. 365-380, 2012.

[13] Y. Zhang, Z. Lin and Q. Liu, “Marine renewable energy in China: Current status and perspectives,” in *Water Science and Engineering Volume 7(3)*, Elsevier, 2014, pp. 288-305.

[14] School of Mechanical, Aerospace and Civil Engineering, University of Manchester, “M4 Wave Power,” October 2014. [Online]. Available: https://www.youtube.com/watch?v=Ga43Zm5exzo. [Accessed January 2020].

[15] M. Folley, “Wave Energy Converter Modelling Techniques Based on Linear Hydrodynamic Theory,” in *Numerical Modelling of Wave Energy Converters: State-of-the-Art Techniques for Single Devices and Arrays*, Elsevier Ltd., 2016, pp. 11-66.

[16] M. D. Esteban, J. S. López-Gutiérrez and V. Negro, “Classification of Wave Energy Converters,” *Recent advances in petrochemical science Volume 2(4),* 2017.

[17] JAMSTEC, “The Mighty Whale,” 2005. [Online]. Available: http://www.jamstec.go.jp/gallery/e/research/system/002.html. [Accessed May 2020].

[18] Wave Dragon Wales Ltd, “Wave Dragon Project - Milla Fjord Site,” April 2020. [Online]. Available: https://tethys.pnnl.gov/project-sites/wave-dragon-project-milla-fjord-site. [Accessed April 2020].

[19] D. Elwood, A. Schacher, K. Rhinefrank, J. Prudell, S. Yim and E. Amon, “Numerical modeling and ocean testing of a direct-drive wave energy device utilizing a permanent

magnet linear generator for power take-off," in *International conference on offshore mechanics and arctic engineering*, ASME, 2009, pp. 817-824.

[20] J. Falnes and P. M. Lillebekken, "Wave-energy research at NTNU," 1997. [Online]. Available: http://folk.ntnu.no/falnes/w_e/index-e.html. [Accessed May 2020].

[21] K. Tarrant and C. Meskell, "Investigation on parametrically excited motions of point absorbers in regular waves," *Ocean Engineering Volume 111,* pp. 67-81, 2016.

[22] V. Boscaino, G. Cipriani, V. D. Dio, V. Franzitta and M. Trapanense, "Experimental Test and Simulations on a Linear Generator-Based Prototype of a Wave Energy Conversion System Designed with a Reliability-Oriented Approach," *Sustainability Volume 9(1),* 2017.

[23] Wello, "Penguin's competitive advantage," 2020. [Online]. Available: https://wello.eu/technology/. [Accessed April 2020].

[24] E. W. P. Group, "Sealed gyro tube," 1979. [Online]. Available: http://www.homepages.ed.ac.uk/v1ewaveg/. [Accessed May 2020].

[25] Specialist Committee on Testing of Marine Renewable Devices, "Recommended Procedures and Guidelines; Wave energy converter model test experiments," in *International Towing Tank Conference*, 2017.

[26] Det Norske Veritas, "DNV-RP-C205: Environmental conditions and environmental loads," 2010.

[27] G. J. Dalton, R. Alcorn and T. Lewis, "Case study feasibility analysis of the Pelamis wave energy convertor in Ireland," in *Renewable Energy Volume 35(2)*, Elsevier, 2010, p. 443–455.

[28] A. A. E. Price, C. J. Dent and A. R. Wallace, "On the capture width of wave energy converters," in *Applied Ocean Research, Volume 31(4)*, Elsevier, 2009, pp. 251-259.

[29] É. Cartan, On Manifolds with an Affine Connection and the Theory of General Relativity, translated by A. Magnon and A. Ashtekar, Napoli: Bibliopolis; Atlantic Highlands, 1986.

[30] J. J. O'Connor and E. F. Robertson, “Marius Sophus Lie,” MacTutor History of Mathematics archive, University of St Andrews., 2000.

[31] T. Frankel, The Geometry of Physics, An Introduction, Cambridge University Press, 2012.

[32] T. Impelluso, “The moving frame method in dynamics: Reforming a curriculum and assessment,” *International Journal of Mechanical Engineering Education Volume 46(2),* pp. 158-191, 2017.

[33] C. Lanczos, The Variational Principles of Mechanics, 4th edition, Dover Publications Inc., 1986.

[34] D. D. Holm, “Geometric Mechanics, Part II: Rotating, Translating, and Rolling,” *Imperial College Press, London,* 2008.

[35] H. Murakami, “A Moving Frame Method for Multi-Body Dynamcis Using SE(3),” *Proceedings of the ASME 2015 International Mechanical Engineering Congress & Exposition IMECE2015, November 13-19, Houston, Texas,* 2015.

[36] S. S. Rao, “Chapter 7 - Numerical Solution of Finite Element Equations,” in *The Finite Element Method in Engineering (Sixth Edition)*, Elsevier Inc., 2018, pp. 257-292.

[37] P. Ricci, “Time-Domain Models,” in *Numerical Modelling of Wave Energy Converters: State-of-the-Art Techniques for single devices and arrays*, London, Orwell Offshore, 2016, pp. 31-66.

[38] DNV GL, “DNVGL-OS-C101, Design of offshore steel structures, general,” 2015.

[39] W. Cummins, “The impulse response function and ship motion,” *Technical Report 1661, David Taylor Model Basin–DTNSRDC,* 1962.

[40] J. C. N. Borge, *The Gaussian Model of Wind-Generated Waves,* UiO. Department of Mathematics, Division of Mechanics, 2016.

[41] H. Gu, P. Stansby, T. Stallard and E. C. Morenoa, “Drag, added mass and radiation damping of oscillating vertical cylindrical bodies in heave and surge in still water,” in *Journal of Fluids and Structures Voume 82*, Elsevier Ltd., 2018, pp. 343-356.

[42] Wamit Inc., “Wamit user manual version 7.0,” 2013. [Online]. Available: http://www.wamit.com/manualupdate/history/V70_manual_old.pdf. [Accessed May 2020].